ФИЗИКА ЭЛЕМЕНТАРНЫХ ЧАСТИЦ И АТОМНОГО ЯДРА
2005. Т. 36. ВЫП. 2

УДК 539.172.3

ALPHA DECAYS OF ${}^{10}_{\Lambda}$Be AND ${}^{10}_{\Lambda}$B HYPERNUCLEI ON THE NUCLOTRON: A CLUE TO SOME PUZZLES IN NONLEPTONIC PROCESSES

Yu. A. Batusov, J. Lukstins, L. Majling, A. N. Parfenov

Joint Institute for Nuclear Research, Dubna

ФИЗИКА ЭЛЕМЕНТАРНЫХ ЧАСТИЦ И АТОМНОГО ЯДРА
2005. Т. 36. ВЫП. 2

УДК 539.172.3

ALPHA DECAYS OF $^{10}_{\Lambda}$Be AND $^{10}_{\Lambda}$B HYPERNUCLEI ON THE NUCLOTRON: A CLUE TO SOME PUZZLES IN NONLEPTONIC PROCESSES

Yu. A. Batusov, J. Lukstins[*], L. Majling*[**], A. N. Parfenov*

Joint Institute for Nuclear Research, Dubna

Hypernuclei are a convenient laboratory to study the baryon–baryon weak interaction and associated effective weak Hamiltonian. The strangeness changing process, in which a Λ hyperon in nuclear matter converts to a neutron with a release of up to 176 MeV, provides a clear signal for a conversion of an s quark to a d quark. It is shown how the nuclear structure aspects of the problem, often an unwelcome detail of calculations attempting to understand a basic two-body $\Lambda N \to NN$ interaction, can be used to pick out components of the effective weak Hamiltonian. It is well known that removing one neutron from ^{9}Be results in ^{8}Be* with a subsequent $\alpha\alpha$ decay. Through this process it would be possible to identify final states of the residual nucleus. So, due to this salient feature of the core nuclei ^{9}Be and ^{9}B, it may be possible to measure the branching fractions $\Gamma^{n(p)}_{\alpha\alpha i}$ for the exclusive decays of the $^{10}_{\Lambda}$Be and $^{10}_{\Lambda}$B hypernuclei. These branching fractions $\Gamma^{n(p)}_{\alpha\alpha i}$ depend on various combinations of four matrix elements, hence their study offers a unique possibility of determining all needed matrix elements of the weak interaction and in such a way localizing the difficulties of the hypernuclear nonmesonic decay puzzle. Recently the Nuclotron accelerator at JINR (Dubna) has supplied the first extracted beam of medium-energy ions. This opens new opportunities of performing hypernuclear experiments. With the new trigger tuned to search for two α-particles, the branching fractions $\Gamma^{n}_{\alpha\alpha i}$ ($^{10}_{\Lambda}$Be) and $\Gamma^{p}_{\alpha\alpha i}$ ($^{10}_{\Lambda}$B) will be measured.

Гиперъядра представляют удобную лабораторию для изучения слабого барион-барионного взаимодействия и связанного с ним слабого гамильтониана. Процесс, при котором Λ-гиперон в ядерной среде превращается в нейтрон с выделением энергии в 176 МэВ, служит четким указанием на конверсию s-кварка в d-кварк. Показано, как можно использовать особенности ядерной структуры (часто затрудняющие расчеты, направленные на описание фундаментального двухчастичного взаимодействия $\Lambda N \to NN$) для определения отдельных компонент эффективного слабого гамильтониана. Хорошо известно, что при удалении из основного состояния ядра ^{9}Be одного нейтрона заселяются несколько состояний ядра ^{8}Be*, которые потом распадаются на две α-частицы. Используя этот процесс, можно однозначно идентифицировать конечные состояния остаточного ядра. Благодаря такой особенности ядер ^{9}Be и ^{9}B можно определить парциальные ширины $\Gamma^{n(p)}_{\alpha\alpha i}$ при эксклюзивном исследовании распадов гиперъядер $^{10}_{\Lambda}$Be и $^{10}_{\Lambda}$B. Эти парциальные ширины являются линейными комбинациями всего четырех матричных элементов слабого взаимодействия, поэтому их изучение предоставляет уникальную возможность определить все необходимые матричные элементы слабого взаимодействия и, таким образом, выявить причину

[*]E-mail: juris@sunhe.jinr.ru

[**]Permanent address: Nuclear Physics Institute, Academy of Sciences of Czech Republic, Řež, Czech Republic.

трудностей, встречающихся при описании безмезонных распадов гиперъядер. На сверхпроводящем ускорителе ОИЯИ — нуклотроне — имеются выведенные пучки ионов промежуточных энергий. Это открывает новые возможности для проведения гиперъядерных экспериментов. При использовании нового триггера, настроенного на срабатывание от двух α-частиц, будут измерены парциальные ширины $\Gamma^n_{\alpha\alpha i}$ ($^{10}_{\Lambda}$Be) и $\Gamma^p_{\alpha\alpha i}$ ($^{10}_{\Lambda}$B).

1. INTRODUCTION. HYPERNUCLEI

The Λ hypernucleus $^{\mathrm{A}}_{\Lambda}Z$ is a bound system of Z protons, $(A-Z-1)$ neutrons and one Λ hyperon. This is one of the best examples of a *nucleus with a new flavor — strangeness*. The lifetime of the hypernucleus is about $2 \cdot 10^{-10}$ s.

Hypernuclei are formed in any reaction of an elementary particle with nucleons of the nucleus in which hyperons are produced. It was discovered by M. Danysz and J. Pniewski in a baloon-flown emulsion stack [1], Fig. 1.

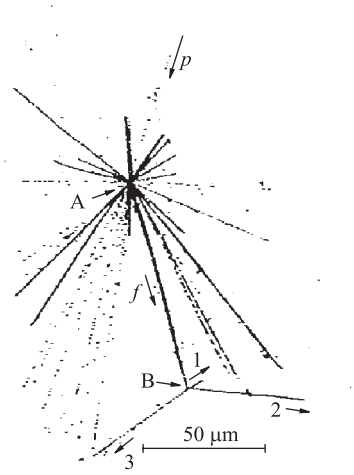

Fig. 1. The first observation of the decay of a hypernucleus: in vertex (A) high-energy cosmic ray (p) colliding with a nucleus of emulsion (silver or bromine) produced hyperfragment (f) decayed in vertex (B). Taken from [1]

For half a century, the strange particles have offered us important clues to the nature of matter and character of the forces which shape the world. Ten years after the discovery of hypernuclei, M. Gell-Mann recognized the $SU(3)$ flavor structure of baryons and mesons, and shortly after realized that it was naturally embodied in the quark model [2].

Hypernuclei not only bring the strangeness to nuclear physics, they provide a convenient tool for obtaining information about the hyperon–nucleon (YN) interaction and explore the full $SU(3)$ symmetry breaking baryon–baryon interaction, strong and weak. In fact, the existing data on ΛN and ΣN strong interaction are extremely sparse and imprecise: production and scattering in the same target are required due to low hyperon beam intensities and short lifetimes. There are several realistic models for the free YN interactions, based on boson exchanges. Well known are YN potentials of the Jülich group [3] constructed along the same guidelines as used in the Bonn NN potential. For many years the Nijmegen group [4] has developed several One-Boson-Exchange Potential models: NSC89, NSC97a-f, ESC00. They have used $SU(3)$ constraints on the coupling constants to fit about 4300 $pp+np$ data on cross sections and variety of spin correlations together with 35 scattering ΛN and ΣN data at low energies. Although

the YN data are both few in number and have rather large errors compared to NN, authors [4] claimed that it was nontrivial to fit the YN data with NN while not allowing YN bound state.

Since the empirical information on YN scattering consists almost exclusively of spin-averaged quantities like total and differential cross sections, the spin structure of the free YN interaction is essentially unknown. Therefore, various models for the YN interaction, which differ widely in their spin (and isospin) dependence, are able to describe the same scattering data. But since the results of hypernuclear structure calculations are sensitive to the spin dependence of the YN interaction, the finite-nuclei YN, G-matrix provides a useful tool for testing the spin structure of various YN interactions [5, 6]. Several authors [7] have analyzed the ΛN effective interaction for p-shell nuclei in terms of five convenient phenomenological parameters $\bar{V}$, Δ, S_Λ, S_N, and T. These parameters can be calculated from G-matrix elements [6].

A very important result was obtained by Miyagawa and Glöckle [8]: the Faddeev equations were solved for the coupled ΛNN-ΣNN system. (For the YN system, various interactions were used, the Jülich $\tilde{A}$ model, and the soft core models of the Nijmegen group NSC89 and NSC97.) Among these models, only NSC89 and NSC97f bind the ${}^{3}_{\Lambda}$H at correct binding energy. The Jülich $\tilde{A}$ interaction cannot generate the bound state. For NN sector, the Paris, Bonn B and Nijmegen 93 interactions has been used, but the results above do not depend on the choice of these potentials. The $\Lambda - \Sigma$ conversion was found to be crucial for the binding energy.

1.1. Status of the Hypernuclear Spectroscopy. As we have already mentioned, hypernuclei were discovered in emulsion where a salient picture, namely «twin stars», corresponding to strong production of the primary hypernucleus and a weak decay of the hyperfragment connected with a path (~ 50 microns) were easily recognized.

The result of a painstaking study combined with laborious analysis of individual events are binding energies of 22 light ($A < 16$) hyperfragments, which form a foundation of hypernuclear spectrocopy [9].

Large scale systematic studies of hypernuclei began with the advent of separated K^- beams, which permitted the use of the counter technique and confirmed a brilliant suggestion of Podgoretskii [10]: instead of hunting down decays of random fragments, to study hypernuclear *production* in strangeness exchange reaction

$$K^- + {}^{A}Z \to {}^{A}_{\Lambda}Z + \pi^-, \quad p_K \approx 530 \text{ MeV}/c, \quad \theta_\pi \approx 0 \qquad (q_\Lambda \approx 0),$$

where the π^- momenta can be used to determine the spectra of hypernuclear resonances.

The pioneering work of groups led by T. Bressani [11] and B. Povh at CERN [12] and R. Chrien at BNL [13] established the existence of hypernu-

clei and allowed a clear assignment of hypernuclear states. The achievements of the hypernuclear spectroscopy using the in-flight (K^-, π^-) reaction stimulated the study of associative production reaction

$$\pi^+ + n \to \Lambda + K^+.$$

The studies began at Brookhaven (USA) [14] and were continued at KEK (Japan) [15]. Owing to a large recoil, this reaction favors population of the states with the maximum angular momentum. The (π^+, K^+) reaction at nonzero angles can be also used to produce polarized hypernuclei [16]. By the electromagnetic production of hypernuclei at TJNAF (USA)

$$e^- + p \to \Lambda + e' + K^+$$

one can access different levels [17]. The different production reactions are complementary and required for a complete study of hypernuclear spectra [18].

From these studies the Λ-nucleus potential was derived and strength of spin–orbit interaction was obtained. It appears that the shell structure of the nucleus is not disrupted by the insertion of the Λ hyperon into the nucleus and the lack of Pauli blocking allows a simple particle-hole structure $\mid l_{j\Lambda}\ l_{jN}^{-1} : J_H \ \rangle$ of the excitations of primary hypernuclei.

In the hypernucleus ground state, the Λ resides in the $1s$ shell and can explore the nuclear interior very deeply. In hypernuclear spectra the deeply-bound single-particle states are clearly seen and demonstrate, in a striking way, the validity of the concept of the shell model orbitals not only in the valence region, but also in the nuclear interior [15].

From the high-resolution γ spectroscopy [19] the information on the ΛN spin–spin, spin–orbit, and tensor interactions is extracted from the splitting of the hypernuclear bound state multiplets. Recently the evidence for the compression of a hypernucleus due to the «glue-like» role of Λ hyperon has been gained also.

Hypernuclei give a new dimension to the traditional world of nuclei (composed of neutrons and protons) by revealing the existence of a new type of nuclear matter and generating new symmetries [20]. There is growing support that hyperons are the first exotic particles to appear in neutron star matter at around twice normal nuclear density, as was recently confirmed within various different models [21]. This is one of the reasons why an intense experimental program is underway or upcoming at BNL, KEK, TJNAF, DAΦNE (Frascati, Italy) [22, 23] and COSY (Germany) [24].

The nonmesonic decay of Λ hypernuclei is of the top physical interest, since it gives an access to the weak decay process $\Lambda N \to NN$ which is achievable only through the observation of the hypernuclear ground state decays. Our purpose is to analyze the characteristics of the Λ-hyperon weak decay in a nuclear medium [25–27].

2. WEAK DECAYS OF HYPERNUCLEI

Hypernuclei are a convenient laboratory to study the baryon–baryon weak interaction and associated effective weak Hamiltonian. The strangeness changing process in which a Λ hyperon converts to a neutron with the release of up to 176 MeV provides a clear signal for the conversion of an s quark to a u- or d quark. The effective operator generally employed to analyze $|\Delta S| = 1$ nonleptonic interactions has the form [28]

$$H_{|\Delta S|=1} = \frac{G_F}{\sqrt{2}} \sin\theta_W \cos\theta_W \sum_i^6 c_i O_i, \tag{1}$$

where θ_W is the weak angle; O_i are the four-quark operators, describing the lowest order W-boson exchange diagrams, gluon radiation correction and also «penguin» diagrams. The coefficients c_i are obtained as solutions of renormalization group equations.

The properties of the free Λ-hyperon decay are well known: it decays nearly 100% via a nonleptonic mode $\Lambda \to N + \pi$:

$$\tau_{\text{free}} = 1/\Gamma_\Lambda = 2.63 \cdot 10^{-10}\ \text{s},$$

$$\Gamma^{\pi^-}/\Gamma_\Lambda = 0.639, \quad \Gamma^{\pi^0}/\Gamma_\Lambda = 0.358, \quad (\Gamma^{\pi^-} + \Gamma^{\pi^0})/\Gamma_\Lambda = 0.997,$$

in agreement with other hyperon decays [29].

Two experimental features of baryonic $|\Delta S = 1|$ decays are noteworthy:

• $\Gamma_{\text{nonlept}} \simeq 400\ \Gamma_{\text{semilept}}$

and

• the empirical $\Delta I = 1/2$ rule: Amplitude $(\Delta I = 1/2) \simeq 20$ Amplitude $(\Delta I = 3/2)$. This suppression exists in both the hyperon and the kaon nonleptonic decays, and, despite a great deal of theoretical work, there is still no simple explanation for its existence.

The energy release in the pionic decay produces a nucleon having a momentum of only some 100 MeV/c (kinetic energy ≈ 5 MeV). Thus, the pionic decay modes are severely inhibited by Pauli blocking.

The dominant mechanism of a hypernuclear decay is not the pionic mode, favoured by free Λ hyperon, but a far more complex $\Lambda + N \to n + N$ process. The 176 MeV energy release in this process corresponds to a final-state nucleon momentum of the order of 400 MeV/c. The total decay width of a hypernucleus, Γ_{tot}, is defined in terms of its mesonic and nonmesonic decay modes

$$\begin{aligned} \tau^{-1} = \Gamma_{\text{tot}} &= \overbrace{\qquad\qquad\qquad}^{\Gamma_m} + \overbrace{\qquad\qquad\qquad}^{\Gamma_{\text{nm}}} \\ &= \overbrace{\Gamma^{\pi^-} + \Gamma^{\pi^0} + (\Gamma^{\pi^+})}^{\Gamma_m} + \overbrace{\Gamma^p + \Gamma^n + (\Gamma^{\text{mb}})}^{\Gamma_{\text{nm}}}; \end{aligned}$$

$\Gamma^{\rm mb}$ as well as Γ^{π^+} are the possible many-body decay modes and are ignored in our discussion.

The main observables which can be measured experimentally and should be confronted with theoretical predictions include the following:

• the hypernuclear lifetime τ;

• the partial decay widths Γ^{π^-}, Γ^{π^0}, Γ^p, and Γ^n;

• the ratio of parity-violating to parity-conserving decay, which is measured via the proton asymmetry in the polarized hypernuclear decay.

The weak interaction at the quark level is short-ranged, involving W and Z exchanges. However, because of the core repulsion, the baryon–baryon effects are modelled in terms of one-meson exchange interaction, not only by the long-range one-pion exchange, but all pseudoscalar (π, η, K) and vector (ρ, ω, K^*) meson exchanges included [30].

2.1. Lifetime of Hypernuclei. The field of the weak decay of Λ hypernuclei has experienced an impressive progress in the last few years [26, 27]. Among weak decay observables, the total decay width (or lifetime) can be measured most accurately [31] and is now available from different experiments. The lifetime measurement can be a starting point for obtaining other observables: Γ^{π^-}, Γ^{π^0}, and Γ^p.

Figure 2 shows the present status of the lifetime results including both the recent measurements [31–36] and calculations [37].

For light hypernuclei of $A \leqslant 5$ there are old emulsion data, «em», [41–43] as well as data obtained on relativistic ion beams, «ri», [44–46]. The most recent and reliable measurements of hypernuclear lifetimes have been carried out at BNL, «$K\pi$», [47–51] and KEK, «πK», [31,33]. The (π^+, K^+) reaction is most suitable for measuring the weak decay of medium and heavy Λ hypernuclei because it can produce the deep-bound state of hypernuclei due to the high-momentum transfer which is as much as 0.4 GeV/c, while the (K^-, π^-) reaction populates preferentially the substitutional states due to the reaction selectivity. In addition, the (π^+, K^+) reaction gives a very clean inclusive spectrum because it is free from the decay of beam particles. This also permits one to estimate the yield of hypernuclear formation in the inclusive spectrum rather precisely. Lifetimes of heavy hypernuclei ($A > 180$) have been studied through the delayed fission induced by the antiproton, «$\bar{p}f$», [52], electron, «ef», [53], and proton, «pf», [32, 34, 35, 54] beams on targets Au, Pb, Bi or U and attributed to hypernuclear production. In [36] the experimental studies of the COSY 13 Collaboration have been summarized and old results commented.

Recent results of the calculation based on the one-pion exchange model are also presented in Fig. 2 (black circles). When model parameters [40] were adjusted to reproduce the nonmesonic decay width of ${}^{12}_{\Lambda}$C reported in [37]; decay rates for heavier hypernuclei were in agreement with the experimental data [31].

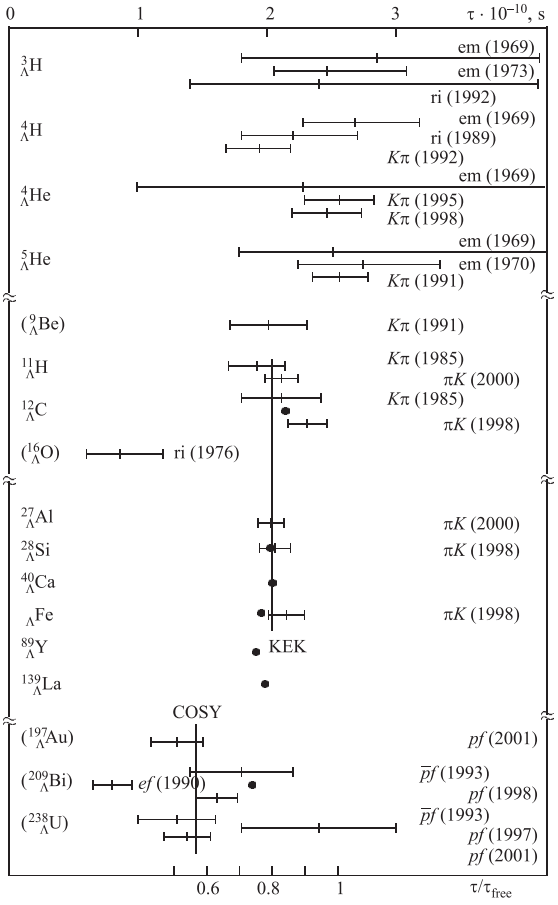

Fig. 2. The mass dependence of hypernuclear lifetime

From the experiments [31] (KEK) it was deduced that the lifetime of Λ hyperon in nuclear matter saturates at $\approx 80\%$ of τ_Λ in free space. But the recent COSY data [36] give a clearly lower value for the lifetimes of heavy hypernuclei.

2.2. The Γ^n/Γ^p Ratio. At present there are four hypernuclei for which the complete set of partial decay rates has been measured. The survey of the results for the Γ^n/Γ^p ratio is displayed in Fig. 3 and Table 1. We see that $0.5 \leqslant (\Gamma^n/\Gamma^p)^{\exp} \leqslant 2$.

The main problem concerning the weak decay of Λ hypernuclei is the disagreement between the theoretical and experimental values for the ratio Γ^n/Γ^p.

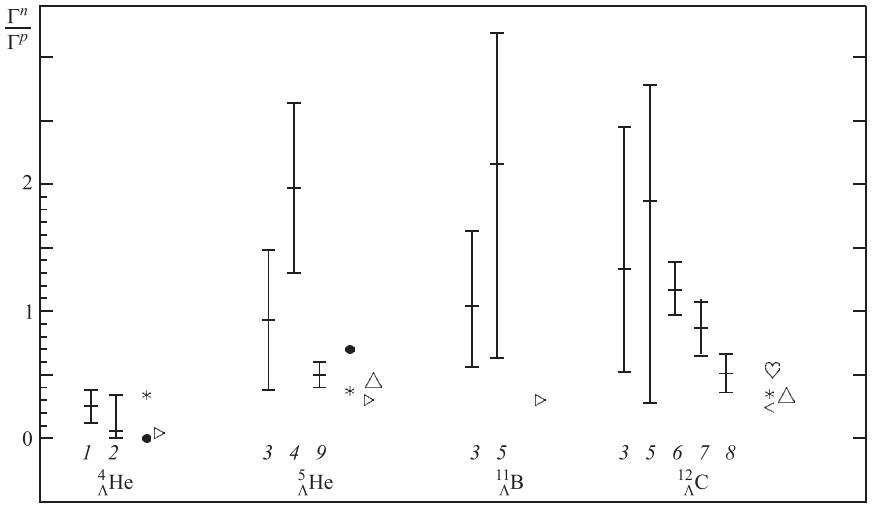

Fig. 3. The survey of the results for the Γ^n/Γ^p ratio. Experiments: *1* — [51]; *2* — [58]; *3* — [48]; *4* — [59]; *5* — [60]; *6* — [61]; *7* — [63]; *8* — [62]; *9* — [69]. Calculations: △ — [66]; ◁ — [67]; ▷ — [65]; ♡ — [38]; ∗ — [64]; • — [56]

Table 1. **Catalogue of the experimental results for the Γ^n/Γ^p ratio**

$^A_\Lambda Z$	$\Gamma_{\rm tot}$	Γ_m		Γ_{nm}		$\frac{\Gamma^n}{\Gamma^p}$	Ref.
		Γ^{π^-}	Γ^{π^0}	Γ^n	Γ^p		
$^4_\Lambda$He	1.07±0.11	0.26±0.03	0.61±0.08	0.04±0.02	0.16±0.02	0.25±0.13	[51]
	$1.03^{+0.12}_{-0.10}$	0.33±0.05	0.53±0.07	$0.01^{+0.04}_{-0.01}$	0.16±0.02	$0.06^{+0.28}_{-0.06}$	[58]
$^5_\Lambda$He	1.03±0.08	0.44±0.11	0.18±0.20	0.20±0.11	0.21±0.07	0.93±0.55	[48]
		0.34±0.04		0.50±0.07		1.97±0.67	[59]
						0.5±0.1	[69]
$^{11}_\Lambda$B	1.37±0.16					$1.04^{+0.59}_{-0.48}$	[48]
		0.23±0.09		0.95±0.17		$2.16^{+1.03}_{-1.53}$	[60]
$^{12}_\Lambda$C	1.25±0.18	$0.052^{+0.063}_{-0.052}$	0.06	1.14±0.20		$1.33^{+1.12}_{-0.81}$	[48]
		0.14±0.10		0.89±0.18		$1.87^{+0.67}_{-1.16}$	[60]
						$1.17^{+0.22}_{-0.20}$	[61]
						0.87±0.23	[63]
						0.51±0.15	[62]

The first theoretical calculations have been based upon a simple impulse approximation, in which the ${}^3S_1$ transition dominates over the ${}^1S_0$ transition (as is found for One-Pion Exchange model (OPE)) but does not contribute to the $n\Lambda \to nn$ process, thus $\Gamma^n \ll \Gamma^p$. In order to solve the Γ^n/Γ^p puzzle, many attempts have been made up to now, but without success. Among these we recall

• the introduction of mesons heavier than the pion in the $\Lambda N \to NN$ transition potential [30, 70];

• the role of the two-nucleon stimulated decay [37, 40, 71];

• the description of the short-range baryon–baryon interaction in terms of quark degrees of freedom [56, 72].

The results of the calculation of decay widths Γ^n and Γ^p in various approaches One-Meson Exchange (OME), Two-Pion Exchange (TPE), Hybrid Quark Mechanism (HQ) are given in Table 2. The result of such an effort is an enlargement of the Γ^n/Γ^p ratio to values 0.4–0.5, lower side of experimental error bars. The experimental data have large uncertainties mainly because Γ^n was not estimated directly, from the neutron measurement, but indirectly as $\Gamma^n = \Gamma_{\rm tot} - \Gamma_m - \Gamma^p - \Gamma^{\rm mb}$. Authors of recent paper [62] carried out the *neutron* measurement, in which the detection energy threshold was reduced to ~ 10 MeV. In order to determine the Γ^n/Γ^p ratio they adopted also the results from the estimation of the effect of final state interaction [73]. After that, the value of Γ^n/Γ^p ratio was obtained to be 0.51 ± 0.15 (stat.). Two experiments aimed in *coincidence measurements* of the two emitted nucleons ($n + p/n + n$) are now in progress at KEK (H. Outa and H. Bhang spokespersons).

Table 2. **Catalogue of the calculated results for the Γ^n/Γ^p ratio**

${}^A_\Lambda Z$	Γ_{nm}		$\frac{\Gamma^n}{\Gamma^p}$	Model	Ref.
	Γ^n	Γ^p			
${}^4_\Lambda$He	0.081	0.222	0.363	TPE	[64]
	0.004	0.214	0.019	HQ	[56]
	0.029	0.478	0.061	OME	[65]
${}^5_\Lambda$He	0.118	0.305	0.386	TPE	[64]
	0.219	0.304	0.720	HQ	[56]
	0.148	0.461	0.320	OME	[65]
	0.099	0.218	0.457	OME	[66]
${}^{11}_\Lambda$B	0.212	0.668	0.318	OME	[65]
${}^{12}_\Lambda$C	0.285	0.775	0.368	TPE	[64]
	0.141	0.413	0.341	OME	[66]
	0.205	0.795	0.258	OME	[65]
	0.277	1.061	0.261	OME	[67]
	0.308	0.571	0.540	OKE	[68]

One has to point out that present experiments cannot identify the final state of the residual $(A-2)$ nucleus in the case of nonmesonic decays

$$ {}^{A}_{\Lambda}Z \to {}^{A-2}Z + n + n \quad \text{and} \quad {}^{A}_{\Lambda}Z \to {}^{A-2}(Z-1) + n + p, $$

and averaging over many nuclear final states has to be performed.

In what follows, we focus our attention on one peculiar case which makes it possible to detect some of these final states [74, 75].

3. SPECTROSCOPY OF $^{9}\mathrm{Be} \to {}^{8}\mathrm{Be} + n$

It is well known that among p-shell nuclei there is a little gulf of instability: nuclei ^{8}Be and ^{9}B (Table 3).

Table 3. **A segment of the chart of light nuclei**

^{9}C 0.13 s	^{10}C 19 s	^{11}C 20 min	^{12}**C** **stab.**
^{8}B 0.77 s	^{9}B	^{10}**B** **stab.**	^{11}**B** **stab.**
^{7}Be 53 d	^{8}Be $\swarrow\ \searrow$ $\alpha \quad \alpha$	^{9}**Be** **stab.**	^{10}Be $1.5 \cdot 10^{6}$ y
^{6}**Li** **stab.**	^{7}**Li** **stab.**	^{8}Li 0.84 s	^{9}Li 0.18 s

We propose to use the unique feature of the ^{9}Be nucleus, namely that after removing a neutron from its ground state several groups of α particles appear from different excited states of a residual nucleus ^{8}Be (see Table 4).

The probabilities of their feeding are governed by spectroscopic factors. The spectroscopic factors are the most important nuclear structure ingredients in transition amplitudes for direct nuclear reactions. We recall that in a typical shell-model calculation of the wave functions for adjacent nuclei, the same radial function is predicted for all overlap with the same lj. This shortcoming of the shell model is also in some sense one of its strong features, i.e., its ability to make rather accurate predictions which do not depend sensitively on the radial form of wave functions.

In our case, spectroscopic factors were extracted from the $^{9}\mathrm{Be}(p,d)^{8}\mathrm{Be}$ reaction: in Ref. 76 (d) (experiment [77] $E_p = 46$ MeV) and in Ref. 78 (e) (experiment [79] $E_p = 156$ MeV). They are compared with predictions of various

Table 4. **Spectrum of ^{8}Be nucleus and neutron spectroscopic factors, S_i^n**

J_i^π	T_i	^{8}Be [82] E_i, MeV	^{8}Be [82] Γ_i, keV	Decay	Calculated E_i, MeV	Calculated S_i^n	Measured S_i^n
0^+	0	0.00	0.007	α	0.00	0.550 (b)	0.67±0.14 (d)
					0.00	0.560 (c)	0.60±0.17 (e)
2^+	0	3.04	1500	α	3.09	0.755 (b)	1.49±0.23 (d)
					3.41	0.720 (c)	1.20±0.21 (e)
4^+	0	11.4	$\sim$3500	α	10.30	0.000 (b)	No fit
					11.29	0.000 (c)	
2^+	1(0)	16.63	108	γ, α	16.76	0.505 (b)	
					15.81	0.515 (c)	1.14±0.19 (d)
2^+	0(1)	16.92	74	γ, α	16.89	0.430 (b)	0.65±0.15 (e)
					14.44	0.475 (c)	
1^+	1	17.64	11	γ, p	17.59	0.223 (b)	0.27±0.05 (d)
					16.89	0.175 (c)	0.10±0.07 (e)
1^+	0	18.15	138	γ, p	18.74	0.070 (b)	0.14±0.04 (d)
					14.98	0.065 (c)	
3^+	(1)	19.07	270	γ, p	18.85	0.180 (b)	
					17.50	0.185 (c)	0.54 ± 0.12 (d)
3^+	(0)	19.24	230	n, p	19.40	0.130 (b)	0.21 ± 0.04 (e)
					16.69	0.070 (c)	

calculations based on the intermediate coupling shell model: Barker [80] (b) or Cohen and Kurath [81] (c). The results are collected in Table 4 and Fig. 4.

We recall that also ^{8}Li nucleus, the product of pick-up of a proton from ^{9}Be, ultimately decays into the $\alpha\,\alpha$ channel.

So, removing one nucleon from ^{9}Be or ^{9}B nuclei results in ^{8}Be*

$$^9\mathrm{Be} \;\rightarrow\; n \;+\; \boxed{^8\mathrm{Be}^* \rightarrow \alpha\alpha}$$

and

$$^9\mathrm{Be} \;\rightarrow\; p \;+\; ^8\mathrm{Li} \quad (\xrightarrow{\beta^-} {}^8\mathrm{Be}^* \rightarrow \alpha\alpha);$$

$$^9\mathrm{B} \;\rightarrow\; p \;+\; \boxed{^8\mathrm{Be}^* \rightarrow \alpha\alpha}$$

and

$$^9\mathrm{B} \;\rightarrow\; n \;+\; ^8\mathrm{B} \quad (\xrightarrow{\beta^+} {}^8\mathrm{Be}^* \rightarrow \alpha\alpha).$$

Due to these specific properties of the core nuclei ^{9}Be *and* ^{9}B, *it may be possible to measure the branching fractions* $\Gamma^{n(p)}_{\alpha\alpha i}$ *for the exclusive decays of*

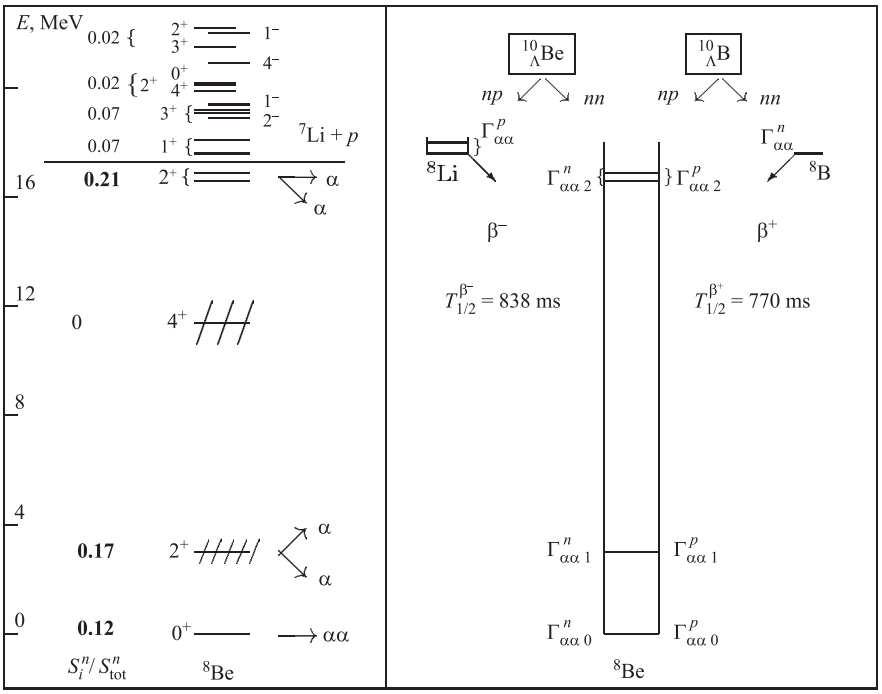

Fig. 4. *a*) Pattern of the ^{8}Be spectra produced in the $^9\mathrm{Be}(p,d)\mathrm{Be}^*$ reaction. *b*) «$\alpha\alpha$ decay» of $^{10}_{\Lambda}$Be and $^{10}_{\Lambda}$B hypernuclei and notation of $\Gamma^{\tau}_{\alpha\alpha i}$

$^{10}_{\Lambda}$Be *and* $^{10}_{\Lambda}$B *hypernuclei to the states of the residual nucleus* ^{8}Be *decaying through the* $\alpha\alpha$ *channel.*

In Fig. 4 the relevant states of $A = 8$ isotopes are displayed, and the notation of the branching fractions $\Gamma^{\tau}_{\alpha\alpha i}$ is explained. The similarity of the structure of $\Gamma^{n}_{\alpha\alpha i}$ ($^{10}_{\Lambda}$Be) and $\Gamma^{p}_{\alpha\alpha i}$ ($^{10}_{\Lambda}$B) is clearly seen. Note that in such a way we can determine not only the partial rate (including the neutron ones), but also an exactly *one-nucleon stimulated* process $\Lambda N \to NN$.

4. PARTIAL DECAY WIDTHS OF $^{10}_{\Lambda}$Be AND $^{10}_{\Lambda}$B

In our contribution to this problem the results summarized recently [70] have been used:

• The one-meson exchange model to describe the $\Lambda N \to NN$ transition was developed in [30]. Pseudoscalar (π, η, K) and vector (ρ, ω, K^*) meson exchanges were included and the $\Delta I = 1/2$ rule at the weak vertex was assumed.

• Following these lines, a full one-meson exchange potential was constructed to study the nonmesonic decay of finite mass hypernuclei and also hadronic weak matrix elements of the form $\langle B'M|H_{\rm weak}|B\rangle$ were implanted into the nucleus with usual many-body shell-model wave functions [83].

• A convenient compact expression for the potential is given by

$$V_{\rm weak}(r) = \sum_i \sum_\alpha V_\alpha^{(i)}(r)\ \hat{O}_\alpha\ \hat{I}_\alpha^{(i)}, \tag{2}$$

where the index i runs over different mesons exchanged ($\pi, \rho, K, K^*, \eta, \omega$); and α, over different spin operators $\hat{O}_\alpha$ (central spin dependent, tensor, PV); the isospin operator $\hat{I}_\alpha^{(i)}$ depends on the meson type. The detailed form of the potential and the explicit values of the coupling constants can be found in [70].

The nonmesonic decay rate $\Gamma_{\rm nm}$ can be written as

$$\Gamma_{\rm nm} = \sum_{\tau=n,p} \Gamma^\tau = \sum_\tau \sum_i \Gamma_i^\tau,$$

where the partial decay width, Γ_i^τ is

$$\Gamma_i^\tau = |\langle \Psi^{A-2}(\{i\}) \otimes \psi^{NN}(JT)|V_{\rm weak} \left| \left[\Psi^{A-1}(\{c\}) \otimes \psi^\Lambda \left(\frac{1}{2}\right)\right]^{\mathcal{J}} \right\rangle \Big|^2 .$$

(We have used the shorthand notation $\{i\} \equiv E_i, J_i, T_i, \tau_i$ for quantum numbers of the excited states of the residual nucleus (see Fig. 3) and $\{c\} \equiv E_c, J_c, T_c, \tau_c$ for quantum numbers of the ground state core nucleus in the decaying hypernucleus.)

It is possible [75] to factorize this expression as

$$\Gamma_i^\tau = \sum_{SJ} G^2_{\mathcal{J}}(\{c\}, \{i\}, \tau LSJ) w_{\ell\tau}^{SJ}, \tag{3}$$

with

$$w_{\ell\tau}^{SJ} = \left| \sum_{L'S'} \langle l_1 l_2 : L'S'JT \mid V_{\rm weak} \mid \tau \ell s_\Lambda : L = \ell SJ\rangle \right|^2 , \tag{4}$$

for matrix elements of the «weak interaction» and $G_{\mathcal{J}}$ for $N\Lambda$-pair fractional parentage coefficient

$$G_{\mathcal{J}}\left(\{c\}, \{i\}, \tau\ell SJ\right) = \sum_j U\left(J_i j \mathcal{J} \frac{1}{2} : J_c J\right)\ U\left(\ell \frac{1}{2} J \frac{1}{2} : jS\right)\ \mathcal{S}_i(\tau\ell j). \tag{5}$$

U are Racah coefficients for three angular momenta recoupling:

$$\begin{aligned} \overbrace{J_i + j}^{J_c} + \frac{1}{2}\,(s_\Lambda) = \mathcal{J} \quad &\rightarrow \quad J_i + \overbrace{j + \frac{1}{2}\,(s_\Lambda)}^{J} = \mathcal{J}, \\ \underbrace{\ell + \frac{1}{2}\,(s_N)}_{j} + \frac{1}{2}\,(s_\Lambda) = J \quad &\rightarrow \quad \ell + \underbrace{\frac{1}{2} + \frac{1}{2}}_{S} = J \end{aligned}$$

and $\mathcal{S}_i(\tau\ell j)$ are spectroscopic amplitudes to separate the nucleon participating in the weak decay from the ground state of the nucleus:

$$\mathcal{S}_i(\tau\ell j) = \sqrt{k}\left(T_i\tau_i\ \frac{1}{2}\tau \,\middle|\, T_c\tau_c\right) g^{E_c\,J_c\,T_c}_{E_i\,J_i\,T_i}\,(\ell j).$$

The $g\,^c_i\,(\ell j)$ is a one-nucleon fractional parentage coefficient in the intermediate coupling:

$$\begin{aligned} g\,^c_i\,(\ell j) = \quad & \sum_{f_c L_c S_c} \ \sum_{f_i L_i S_i} \quad a^{E_c\,J_c\,T_c}_{f_c L_c S_c}\ a^{E_i\,J_i\,T_i}_{f_i L_i S_i} \\ & \begin{pmatrix} L_i & S_i & J_i \\ \ell & \frac{1}{2} & j \\ L_c & S_c & J_c \end{pmatrix} \\ & \langle \ell^k[f_c] L_c S_c T_c \ \{|\ \ell^{k-1}[f_i] L_i S_i T_i\rangle. \end{aligned} \tag{6}$$

The coefficients $a^{E_c\,J_c\,T_c}_{f_c L_c S_c}$, $a^{E_i\,J_i\,T_i}_{f_i L_i S_i}$ result from the shell-model Hamiltonian diagonalization, (e.g., Barker [80], or Cohen and Kurath [81]), $9j$-symbol is used to transform the wave function from jj to LS coupling and $\langle \ell^k\{c\}\{|\ \ell^{k-1}\{i\}\rangle$ is a standard fractional parentage coefficient in the LS coupling.

There are only four $|p_j s_\Lambda : J\rangle$ states: $p_{\frac{1}{2}} s_\Lambda$ $J = 0$ & 1 and $p_{\frac{3}{2}} s_\Lambda$ $J = 1$ & 2, or, in a LS-coupling scheme, $^1P_1$, $^3P_0$, $^3P_1$, and $^3P_2$. Hence, partial nonmesonic decay widths of any $1p$-shell hypernucleus for transitions into natural parity states are linear combinations of four matrix elements only.

From Eq. (4) one can easily see that partial decay widths corresponding to different J_i values are determined by quite definite and different combinations of matrix elements $w^{SJ}_{1\tau}$. The coefficients of these combinations for our case $J_c = \dfrac{3}{2}$, $\mathcal{J} = 1$ are given in Table 5. As a result, in an ideal case when the transitions to final states with $J_i = 0,\ 1,\ 2$, and 3 are observed, one can unambiguously determine all four matrix elements $w^{SJ}_{\ell\tau}$. The nuclear residual interaction accounted by the many-particle shell model influences the quantities $g_{\frac{1}{2}}$ and $g_{\frac{3}{2}}$.

Table 5. $g_j U\left(J_i j \mathcal{J} = 1\,\frac{1}{2} \,:\, J_c = \frac{3}{2}\,J\right)\; U\left(L = 1\,\frac{1}{2}\,J\,\frac{1}{2} \,:\, jS\right)$

J_i	$^{2S+1}P_J$			
	$^3P_0$	$^1P_1$	$^3P_1$	$^3P_2$
0		$\sqrt{\frac{2}{3}}\,g_{\frac{3}{2}}$	$\sqrt{\frac{1}{3}}\,g_{\frac{3}{2}}$	
1	$\sqrt{\frac{2}{3}}\,g_{\frac{1}{2}}$	$-\sqrt{\frac{1}{9}}\,g_{\frac{1}{2}}$ $+\sqrt{\frac{5}{9}}\,g_{\frac{3}{2}}$	$\sqrt{\frac{2}{9}}\,g_{\frac{1}{2}}$ $+\sqrt{\frac{5}{18}}\,g_{\frac{3}{2}}$	$\sqrt{\frac{1}{6}}\,g_{\frac{3}{2}}$
2		$-\sqrt{\frac{1}{3}}\,g_{\frac{1}{2}}$ $+\sqrt{\frac{1}{3}}\,g_{\frac{3}{2}}$	$\sqrt{\frac{2}{3}}\,g_{\frac{1}{2}}$ $+\sqrt{\frac{1}{6}}\,g_{\frac{3}{2}}$	$\sqrt{\frac{1}{2}}\,g_{\frac{3}{2}}$
3				$1\,g_{\frac{3}{2}}$

These matrix elements $w^{SJ}_{\ell\tau}$ will open up a possibility of extending the popular [84] and useful phenomenological model by Block & Dalitz [85] up to p-shell hypernuclei, see below Sec. 7. Together with the data for $\Gamma^{\tau}_{\rm tot}$ it would be possible to disentangle the contribution of the P partial wave [86]. The study of $\Gamma^{\tau}_{\alpha\alpha i}$ offers a unique possibility of determining all needed matrix elements of the weak interaction [70] and resolve the puzzle of the neutron-to-proton induced decay rates Γ^n/Γ^p [26].

5. EXPERIMENTAL POSSIBILITIES

The branching fractions $\Gamma^{\tau}_{\alpha\alpha i}$ can be determined through detection of tagged α particles. Such tagged α particles were recognized as «hammer tracks» in the emulsion and were efficiently used to identify ${}^{8}_{\Lambda}$Li ($\rightarrow \pi^{-}{}^{8}$Be*) [87].

A high-statistics study of the production, decay, and lifetime of the p-shell hypernuclei ${}^{7}_{\Lambda}$Li, ${}^{9}_{\Lambda}$Be, and ${}^{10}_{\Lambda}$B is one of the main physics priorities of the experimental programme for FINUDA [23]. So, there we can obtain $\sigma_{\rm prod}({}^{10}_{\Lambda}{\rm B})$ as well as $\Gamma^{n}_{\rm tot}({}^{10}_{\Lambda}{\rm B})$ and $\Gamma^{p}_{\rm tot}({}^{10}_{\Lambda}{\rm B})$.

There is some hope [74] that it will be possible to use *photoemulsion* there and gain $\Gamma^{p}_{\alpha\alpha\,2}({}^{10}_{\Lambda}{\rm B})$, $\Gamma^{p}_{\alpha\alpha\,1}({}^{10}_{\Lambda}{\rm B})$, $\Gamma^{n}_{\alpha\alpha\,1}({}^{10}_{\Lambda}{\rm Be})$, $\Gamma^{n}_{\alpha\alpha\,2}({}^{10}_{\Lambda}{\rm Be})$, as well as $\Gamma^{n}_{\alpha\alpha}({}^{10}_{\Lambda}{\rm B})$ and $\Gamma^{p}_{\alpha\alpha}({}^{10}_{\Lambda}{\rm Be})$ exploring unique tracks ^{8}Li $\stackrel{\beta^-}{\rightarrow}\,\alpha\alpha$ and ^{8}B $\stackrel{\beta^+}{\rightarrow}\,\alpha\alpha$. However, there is no experience of using photoemulsion in hypernuclear experiments at a collider yet.

Recently, the first hypernuclear spectroscopy experiment using the $^{12}\mathrm{C}(e,e'K^+)^{12}_{\Lambda}\mathrm{B}$ reaction has been successfully performed at TJNAF [88]. In this reaction, the primary hypernucleus is produced with a large momentum. To detect the delayed α particles, it was proposed to use a large acceptance (2π sr) detector based on low-pressure multiwire proportional chambers and low-pressure multistep chambers [89]. According to preliminary estimates, detection of α particles with $E_\alpha = 8$ MeV should be possible. So, $\Gamma^n_{\alpha\alpha 2}(^{10}_{\Lambda}\mathrm{Be})$ and $\sigma_{\mathrm{prod}}(^{10}_{\Lambda}\mathrm{Be})$ could be determined.

Table 6. **Partial decay widths and full one-nucleon induced decay widths**

	p-shell proton (w^{SJ}_{1p})								s-shell proton			
$\Gamma^p_{\alpha\alpha}(^{10}_{\Lambda}\mathrm{Be}) = 0.441$	w^{01}_{1p}	+0.491	w^{11}_{1p}	+0.548	w^{12}_{1p}	+0.157	w^{10}_{1p}					
$\Gamma^p_{\alpha\alpha 2}(^{10}_{\Lambda}\mathrm{B}) = 0.096$	w^{01}_{1p}	+0.520	w^{11}_{1p}	+0.439	w^{12}_{1p}							
$\Gamma^p_{\alpha\alpha 1}(^{10}_{\Lambda}\mathrm{B}) = 0.388$	w^{01}_{1p}	+0.051	w^{11}_{1p}	+0.408	w^{12}_{1p}							
$\Gamma^p_{\alpha\alpha 0}(^{10}_{\Lambda}\mathrm{B}) = 0.412$	w^{01}_{1p}	+0.206	w^{11}_{1p}									
$\Gamma^p_{\mathrm{tot}}\ (^{10}_{\Lambda}\mathrm{B}) = 1.187$	w^{01}_{1p}	+0.822	w^{11}_{1p}	+1.248	w^{12}_{1p}	+0.117	w^{10}_{1p}	+0.354	w^{00}_{0p}	+1.271	w^{11}_{0p}	
$\Gamma^p_{\mathrm{tot}}\ (^{10}_{\Lambda}\mathrm{Be}) = 0.569$	w^{01}_{1p}	+0.535	w^{11}_{1p}	+0.981	w^{12}_{1p}	+0.165	w^{10}_{1p}	+0.437	w^{00}_{0p}	+1.313	w^{11}_{0p}	
	p-shell neutron (w^{SJ}_{1n})								s-shell neutron			
$\Gamma^n_{\alpha\alpha}(^{10}_{\Lambda}\mathrm{B}) = 0.141$	w^{01}_{1n}	+0.489	w^{11}_{1n}	+0.505	w^{12}_{1n}							
$\Gamma^n_{\alpha\alpha 2}(^{10}_{\Lambda}\mathrm{Be}) = 0.096$	w^{01}_{1n}	+0.520	w^{11}_{1n}	+0.439	w^{12}_{1n}							
$\Gamma^n_{\alpha\alpha 1}(^{10}_{\Lambda}\mathrm{Be}) = 0.388$	w^{01}_{1n}	+0.051	w^{11}_{1n}	+0.408	w^{12}_{1n}							
$\Gamma^n_{\alpha\alpha 0}(^{10}_{\Lambda}\mathrm{Be}) = 0.412$	w^{01}_{1n}	+0.206	w^{11}_{1n}									
$\Gamma^n_{\mathrm{tot}}\ (^{10}_{\Lambda}\mathrm{Be}) = 1.187$	w^{01}_{1n}	+0.822	w^{11}_{1n}	+1.248	w^{12}_{1n}	+0.117	w^{10}_{1n}	+0.354	w^{00}_{0n}	+1.271	w^{11}_{0n}	
$\Gamma^n_{\mathrm{tot}}\ (^{10}_{\Lambda}\mathrm{B}) = 0.569$	w^{01}_{1n}	+0.535	w^{11}_{1n}	+0.981	w^{12}_{1n}	+0.165	w^{10}_{1n}	+0.437	w^{00}_{0n}	+1.313	w^{11}_{0n}	

Table 7. **Sources of $\Gamma^n_{\alpha\alpha i}(^{10}_{\Lambda}\mathrm{Be})$ and $\Gamma^p_{\alpha\alpha i}(^{10}_{\Lambda}\mathrm{B})$**

$^{10}_{\Lambda}\mathrm{B}$				$^{10}_{\Lambda}\mathrm{Be}$			
$\Gamma^p_{\alpha\alpha 2}$	em	c2	DN	$\Gamma^n_{\alpha\alpha 2}$	em	C1	DN
$\Gamma^p_{\alpha\alpha 1}$	em		DN	$\Gamma^n_{\alpha\alpha 1}$	em		DN
$\Gamma^p_{\alpha\alpha 0}$				$\Gamma^n_{\alpha\alpha 0}$			
$\Gamma^n_{\alpha\alpha}$	em			$\Gamma^p_{\alpha\alpha}$	em		
Γ^p_{tot}	F1			Γ^n_{tot}	f2		
Γ^n_{tot}	F1			Γ^p_{tot}	f2		
σ_{prod}	F1	c2		σ_{prod}	f2	C1	

Notation

F1:	$^{10}\mathrm{B}(K^-,\pi^-)^{10}_{\Lambda}\mathrm{B}$	f2:	$^{10}\mathrm{B}(K^-,\pi^0)^{10}_{\Lambda}\mathrm{Be}$
c2:	$^{10}\mathrm{B}(e,e'K^0)^{10}_{\Lambda}\mathrm{B}$	C1:	$^{10}\mathrm{B}(e,e'K^+)^{10}_{\Lambda}\mathrm{Be}$
em:	emulsion	DN:	Rel. Ion Coll.

The points of production and decay of *relativistic hypernuclei* are separated by many centimeters (instead of some microns in classical emulsion experiments) and this situation offers a great advantage [90]: a possibility of observing and studying independently the production and decay of hypernuclei. With the new trigger tuned to search for two tagged α particles, $\Gamma^{n}_{\alpha\alpha\,2}(^{10}_{\Lambda}\mathrm{Be})$, $\Gamma^{n}_{\alpha\alpha\,1}(^{10}_{\Lambda}\mathrm{Be})$, $\Gamma^{p}_{\alpha\alpha\,2}(^{10}_{\Lambda}\mathrm{B})$, and $\Gamma^{p}_{\alpha\alpha\,1}(^{10}_{\Lambda}\mathrm{B})$ could be measured at the Nuclotron (Tables 6, 7).

6. RELATIVISTIC HYPERNUCLEI

In some way, the experiments with medium energy (4–6 GeV per nucleon or GeV/a.m.u. — atomic mass unit or GeV/u) hypernuclei, which have been carried out at the Synchrophasotron beams or are suggested for the new accelerator Nuclotron at Dubna, can be specified as a new item in the list of experimental methods. Indeed, in all experiments (except Dubna) hypernuclei are produced in different processes of the target excitation. The most typical is the recoilless strangeness transfer method offered by M. Podgoretsky [10]. The common feature of all experiments of such a type is that momenta of produced hypernuclei are low and they decay practically at the production point inside the target. On the contrary, in the Dubna experiments the energy of hypernuclei is only slightly lower than that of the beam nuclei and a significant part of hypernuclei decay far beyond the production target.

It should be stressed that hypernuclear production is a process of low transferred momentum. The higher momentum is transferred to a target nucleus, the lower is probability for the nucleus to be survived in the interaction and to be transformed into a «nucleus with embedded Λ hyperon» as hypernuclei were defined in an excellent review by H. Bandō, T. Motoba and J. Žofka [18]. Obviously, high energy interactions are not the best source for the production of hypernuclei of strangeness equal to 1 and it is natural that colliders at CERN or Brookhaven do not produce hypernuclei with A number of the order of 10 at all. Indeed, the calculations by Baltz et al. [93] predict dramatic decrease of the hypernuclear production cross section with increase of the mass number. For example, it was expected that just at AGS energy in Au + Au collision the $^{4}_{\Lambda}$H production cross section should be of an order lower than that for the $^{3}_{\Lambda}$H production. On the contrary, if to use the medium energy nuclear beams (3–10 GeV per a nucleon, Synchrophasotron, Nuclotron) to produce hypernuclei of the mass number close to the initial beam, the production cross section depends on A number in quite a different way in consequence with the structure of nuclei (see calculations [94–96] and experiment [97]). At the Synchrophasotron beam the experimentally measured $^{4}_{\Lambda}$H production cross section [45] was much higher than that for $^{3}_{\Lambda}$H. Anyway, there is a possibility to have a reasonable rate of hyper-

nuclear production by means of the beam nuclei excitation at medium energies. Hypernuclear experiments in such beams will be analyzed in detail.

If hypernuclei are produced in a target and, consequently, decay at the production point, experimentalists study (transferred) momentum spectra of kaons or pions — spectators of hypernuclear production — in order to extract data on hypernuclear production and excitation levels. In such an approach the hypernuclei are identified as one or several peaks above the continuum distribution of background interactions. Peaks should be located at specific transferred momentum values which correspond to the mass of hypernucleus at the ground state or excitation levels. In another approach the spectra of decay products — pions, protons and, recently in a few experiments, of γ rays — are investigated to find out the decay of hypernuclei and to collect data on hypernuclear properties. However, there is no method which can be nominated as universal and absolutely adequate for hypernuclear physics to provide a complete set of the data and to solve all the problems. For example, it seems that γ spectroscopy is a very powerful instrument because the resolution is so high that allows one to investigate 100 keV splitting of excitation levels [19] while mesonic spectroscopy is limited at 1 MeV resolution. But, on the other hand, the γ spectroscopy offers rather low statistics. Also it should be noted that hypernuclear spectroscopy generally provides the data which are necessary to push forward the theory of the hyperon–nucleon strong interactions but does not inform about the weak ΛN interactions.

6.1. Relativistic Hypernuclei. In our opinion, the investigation of hypernuclei produced due to excitation of the nuclei accelerated up to a few GeV energy, provides possibilities and approaches which can be useful, moreover, sometimes it gives a unique way to solve some tasks. If a hypernucleus is produced in the excitation process of an accelerator beam nucleus, one has a hypernucleus with a momentum slightly lower than the beam momentum (at the Nuclotron experiments it means the momentum of 5–7 GeV/c per nucleon, see Fig. 7). The lifetime of this hypernucleus in the laboratory frame is multiplied with the Lorentz factor (for the Nuclotron beams the value is approximately equal to 7) and the decay points are distributed in quite a large distance beyond the production target. In such experiment the lifetime can be measured as the distribution of decay points. For example, the lifetime of 200 ps is equal to a decay range of approximately 40 cm distance. If the high energy hypernuclei decay at a distance large enough, one can say that we have a hypernuclear beam which allows one to investigate the properties of hypernuclear production (cross sections) and to study interactions of this beam by inserting absorbers as it is suggested for one of the Dubna project experiments [103, 104]. The magnetic field can be used instead of absorbers in order to search for polarization effects. Since the accelerator and beam transport system give a possibility to produce beams of specified isotopes one has an additional chance to identify hypernuclei. For example, if the ^{10}B or ^{10}C beam

is used to produce hypernuclei, there is no doubt that the investigated sample does not contain hypernuclear isotopes with mass number 11 or higher. If one registers hypernuclear decays beyond the production target in a vacuum volume as it is suggested for the future Nuclotron experiments, then the hypernuclear sample contains no background admixture and event-by-event analysis is possible if necessary.

It should be noted that the method can be used as a complementary one. For example, it allows one to measure the hypernuclear lifetime with excellent accuracy and without systematic errors. If the lifetime of a hypernucleus is measured by using the method elaborated in the Dubna experiments, the result can be applied to calibrate the experimental setup based on the method of prompt measuring the time delay between the production and decay, because one can estimate the value of systematic errors of timing techniques and use this correction for the whole set of experimental data.

An idea to use the beams of nuclei accelerated in Dubna and Berkeley up to medium energies (2–4 GeV per nucleon) for hypernuclear experiments, arose simultaneously with these beams. Since there were no calculations on the hypernuclear production cross sections, some very crude speculations suggested a copious production rate. A very high production cross section of $^{16}_{\Lambda}$O was reported in [46] in the first (very short) Berkeley experiment. Later, the calculations based on the coalescence model [94–96] and Dubna experiments [45] have shown rather lower production cross sections, namely in the 0.05–2.5 μb region for a large set of production reactions in He–Ne beams. Quite a different approach of Kaptari and Titov [99] gave the result of the same order (but very different and strong energy dependence). Considering the Berkeley experiment [46] it seems that the hypernuclei production rate was overestimated due to rather poor identification of hypernuclei. Indeed, there was no event-by-event background separation to skip the beam nuclei fragmentation in spark chamber electrodes. One cannot be sure that the $^{16}_{\Lambda}$O lifetime measurement in the experiment was not distorted by the background admixture either. However, in Dubna it was shown later [97] that the identification problems can be solved for a part of decay modes. On the other hand, it should be noted that the most difficult problem of the hypernuclear experiments in nuclei beams is the trigger problem. Indeed, the background can be eliminated quite well if to use detectors which allow one to identify hypernuclear decays, for example, if hypernuclei decay vertices are located with high accuracy and effective mass values are measured. Moreover, as it has been mentioned above, if one is sure that the decay vertex is located in vacuum, there is no background admixture. Meanwhile, the trigger used in the Berkeley experiment, was tuned to register production and decay of low-energy K meson. This trigger can enrich the sample of triggered interactions with strange particle production but it is not effective enough to show that hypernucleus has been produced and to suppress background significantly. Different tests of this trigger in Dubna have

shown that very often the decay of K^+ meson is simulated by $\pi \to \mu$ chain what is an additional background source.

6.2. Previous Dubna Experiments. Quite another type of the trigger was elaborated in Dubna which allowed one to carry out hypernuclear experiments [44, 45, 97] where hypernuclear production cross sections (see Table 8) and lifetimes of ${}^{3}_{\Lambda}$H and ${}^{4}_{\Lambda}$H were measured successfully in the Synchrophasotron nuclear (^{3}He, ^{4}He, ^{6}Li) beams by using the streamer chamber.

Table 8. **Hypernuclear production cross sections measured in the Synchrophasotron experiment [45]**

Beam	Hyper-nuclei	Energy, GeV/nucleon	Cross sections, μb	
			Theory	Experiment
^{3}He	${}^{3}_{\Lambda}$H	5.14	0.03	$0.05^{+0.05}_{-0.02}$
^{4}He	${}^{3}_{\Lambda}$H	3.7	0.06	< 0.1
	${}^{4}_{\Lambda}$H	2.2	0.08	< 0.08
		3.7	0.29	$0.4^{+0.4}_{-0.2}$
^{6}Li	${}^{3}_{\Lambda}$H	3.7	0.09	$0.2^{+0.3}_{-0.15}$
	${}^{4}_{\Lambda}$H	3.7	0.2	$0.3^{+0.3}_{-0.15}$
^{7}Li	${}^{7}_{\Lambda}$Li	3.0	0.11	< 1
	${}^{6}_{\Lambda}$He	3.0	0.25	< 0.5

Let us look at the layout of the first Dubna experiment (Fig. 5) to understand the idea of the original trigger and to analyze some properties of the experimental method in detail. ^{4}He beam (energy 3.6 GeV per nucleon) hits the polyethylene target (T) which was inserted between the streamer chamber electrodes at a distance of 10 cm in front of the beam entrance window. The length of the target was chosen using the formula elaborated by S. Khorozov [98]:

$$w_t = \frac{\lambda\mu_1}{\lambda(\mu_2 - \mu_1) + 1}(\mathrm{e}^{-\mu_1 L} - \mathrm{e}^{-L(\mu_2 + 1/\lambda)}). \tag{7}$$

Here w_t is a probability that a hypernucleus produced in the target will leave the target without decaying and inelastic interaction; L — the target length; $\lambda = pc\tau/m$ — lifetime of hypernucleus expressed as a distance between the production and decay points (p — momentum, m — mass, τ — lifetime of hypernucleus, c — velocity of light); μ_1, μ_2 — linear absorption coefficients for the beam nuclei and the hypernuclei ($\mu = \rho\sigma N_A/A$, where ρ — target density, σ — absorption cross section for the beam nuclei or the hypernuclei, correspondingly, N_A — Avogadro number, A — atomic number of the target). The optimal target length at the energy of 4 GeV per nucleon was 10–15 cm for carbon or polyethylene.

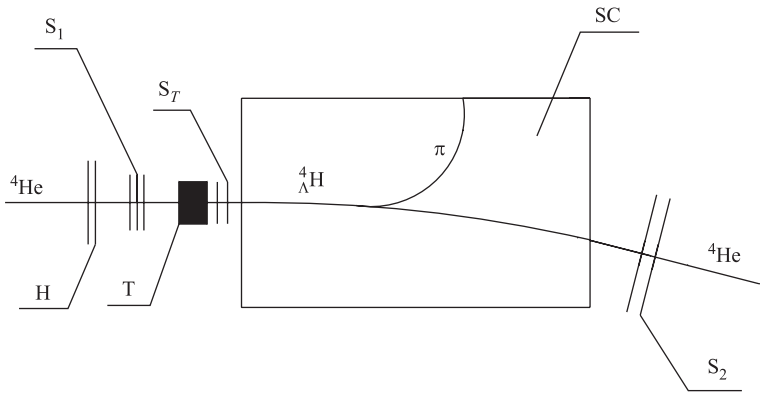

Fig. 5. Hypernuclear experiment with the 2-m streamer chamber (SC). Hodoscopes (H) were used to adjust the beam, trigger counters were used to measure the charge of beam nuclei ^{4}He (S_1), hypernuclei $^4_\Lambda$H (S_T), and daughter nuclei ^{4}He (S_2). The polyethylene target (T) placed at 10 cm in front of the streamer chamber entrance window

Two scintillation counters (S_T) placed between the target and the chamber electrodes and the entrance window, were used to measure the charge of the produced hypernucleus (equal to 1 for $^4_\Lambda$H). If one takes into account that the streamer chamber high voltage peak value was of 500 kV and the magnetic field of the order of 10000 Gs, it is obvious that rather difficult technical problems have been solved to obtain a good resolution of the scintillation counters. Two-meter streamer chamber (SC) was long enough to register all hypernuclei decays beyond $\sim$20 cm of the target and to measure the momentum of a negative pion within errors of 1% and the momentum of a daughter nucleus with errors of 5%. The decay vertex position was measured with an accuracy of a few mm. Scintillation counters S_2 beyond the streamer chamber were used to register ^{4}He — the daughter nuclei of the $^4_\Lambda$H hypernuclei. Trajectories of the daughter nuclei ^{4}He and prompt beam nuclei ^{4}He (which escaped interactions in the target) were slightly different due to the corresponding momentum difference. The position and size (40$\times$25 cm) of the counters S_2 were chosen to have practically 100% geometrical efficiency for the daughter nuclei and to have a minimal overlap with the beam spot. Scintillation counters S_1 and H were applied for the beam control purposes. Hypernuclear production (2) and decay (3) in the experiment can be described by the chain of reactions:

$$^4\mathrm{He} + A \rightarrow {}^4_\Lambda\mathrm{H}\ ({}^3_\Lambda\mathrm{H}) + \ldots, \tag{8}$$

$${}^4_\Lambda\mathrm{H}\ ({}^3_\Lambda\mathrm{H}) \rightarrow {}^4\mathrm{He}\ ({}^3\mathrm{He}) + \pi^-. \tag{9}$$

The accuracy of the momentum measurement was high enough to have unambiguous hypernuclei identification (see effective mass distribution in Fig. 6, few background events — charge exchange reaction on neon gas filling the streamer chamber — are far outside the borders of the displayed histogram). On the other hand, it was necessary to separate ${}^{3}_{\Lambda}\mathrm{H}$ and ${}^{4}_{\Lambda}\mathrm{H}$ events because trigger conditions were similar for both the processes. This problem in the experiment was solved very simply. While hypernuclei energy was slightly lower than 3.5 GeV per nucleon and the energy of daughter nuclei was just lower, momenta of ${}^{4}\mathrm{He}$ and ${}^{3}\mathrm{He}$ were concentrated around corresponding 4×4 and 3×4 GeV/c values and could be clearly separated by the streamer chamber momentum measurement. It should be noted that if the experiment was tuned to register ${}^{4}_{\Lambda}\mathrm{H}$, the scintillation counters C were installed to provide 100% efficiency for ${}^{4}_{\Lambda}\mathrm{H}$, while a part of ${}^{3}_{\Lambda}\mathrm{H}$ daughter nuclei (${}^{3}\mathrm{He}$) were missed by the counters C.

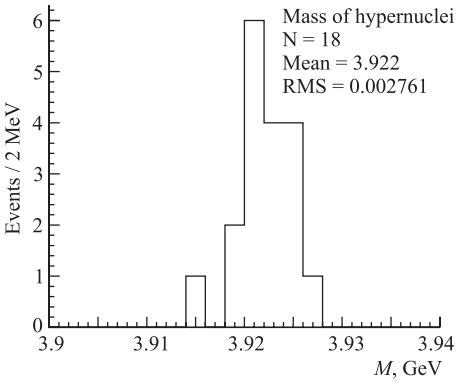

Fig. 6. Effective mass distribution of ${}^{4}_{\Lambda}\mathrm{H}$ hypernuclei

Trigger electronics analyzed the signals depending on the charge value of hypernuclei and daughter nuclei in case of a pionic decay channel of hypernuclei. If the charge value of the hypernucleus is equal to Z, then the charge of the daughter nucleus is $Z+1$ for this decay mode. For example, in case of the He beam, analyzed above, hydrogen hypernuclei were produced with $Z=1$ and, of course, $Z+1=2$. The corresponding response of scintillation or Cherenkov counter is proportional to Z^2 and $(Z+1)^2$. The main advantage of the chosen approach is that the background can be suppressed to any desired level by means of several filters. Indeed, $Z+1$ signal cannot be simulated by fragments of a beam nucleus while one can install counters with the resolution good enough to separate signals proportional to Z^2 and $(Z+1)^2$. In the first experiments a significant part of the beam nuclei did not hit detector C for daughter nuclei because of different trajectories in the magnetic field. Naturally, the better is the resolution of detectors used to measure Z values of beam particles, the better is the background suppression. However, if the resolution of a single detector measuring Z value is not good enough and the signal overlaps with the signal from $Z+1$ detector, one can use two (three) detectors to measure each value with thresholds eliminating the signal mixing. In the result, it is possible to suppress the background to the level 10^{-5} or, probably, up to 10^{-6} without significant reduction of the efficiency of the hypernuclear trigger, at least, for the light and medium mass nuclei.

For example, in the previous Dubna experiment the trigger was tuned to fire the streamer chamber 0.2–0.3 times per accelerator cycle to avoid 2 triggers per cycle (the streamer chamber could not response to the second trigger and to register this second event). Thus, approximately 10^{-4} He interactions in the target triggered the streamer chamber. Of course, all these interactions stimulated the background triggers because the hypernuclear events were observed with a frequency lower than one event per day. On the other hand, it was obvious that the trigger frequency could be reduced by an order quite easy but such reduction was not necessary or useful due to possible reduction of the hypernuclear registration efficiency. Different detectors can be used to measure coincidence of the Z and $Z + 1$ signals. For example, scintillation counters were used in the first Dubna experiment while Cherenkov counters are proposed for the future experiments. The reason is that in the first experiment long (2.5 m) light pipes were used to collect light from counters B near the streamer chamber. The resolution of the Cherenkov counter under such conditions is lower than of the scintillation counter. In the next experiment phototubes can be located near the beam and Cherenkov counters are preferable in the case.

On the other hand, the geometrical efficiency of the trigger can be very close to 100%. Hypernuclei are produced in processes with low transferred momentum thus the transverse momentum of a hypernucleus is small according to its few GeV/c longitudinal momentum. The decay energy for the pionic channel is 38 MeV. In the result, hypernuclei as well as daughter nuclei are emitted at small angles. For example, in the Dubna experiment when the beam energy was 3.6 GeV per nucleon, the total angular spread of the registered daughter nuclei was of the order of 10 mrad. At 6 GeV per nucleon the secondary particles will be just

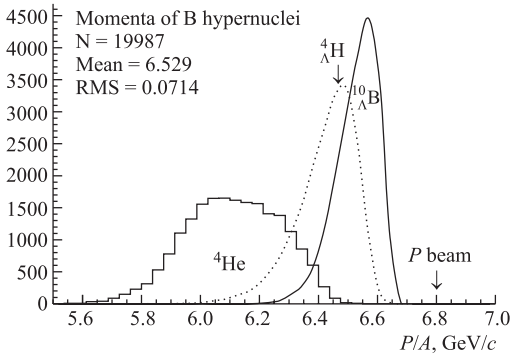

Fig. 7. Calculated momentum per nucleus (P/A) distributions for $^{4}_{\Lambda}$H (dotted line) and $^{10}_{\Lambda}$B (solid line) hypernuclei produced in the Nuclotron highest energy nuclear beams (6.8 GeV/c per nucleon). The histogram reproduces momenta of ^{4}He — daughter nuclei of $^{4}_{\Lambda}$H

more focused which helps one to produce the high quality and acceptance trigger detectors. Our calculations of the expected momentum and angular distributions for the 6 GeV hypernuclei are presented in Figs. 7 and 8. Since approximately the same energy should be transferred to produce Λ, any of 10 boron nucleons

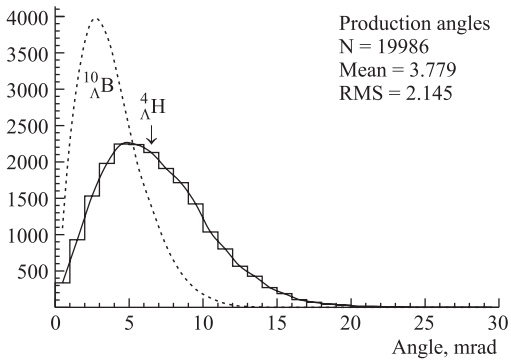

Fig. 8. Calculated distributions of $^{4}_{\Lambda}$H (solid line) and $^{10}_{\Lambda}$B (dotted line) hypernuclei production angles. The histogram shows that the angular distribution of the ^{4}He — daughter nuclei and of $^{4}_{\Lambda}$H are similar

share the less momentum value than 4 helium nucleons therefore the mean $^{10}_{\Lambda}$B momentum (6.53 GeV/c) is slightly higher than that (6.43 GeV/c) of $^{4}_{\Lambda}$H.

Analyzing the approach and results of the Dubna experiment one can see several advantages: unambiguous identification of hypernuclei, low background and good efficiency of the trigger tuned to register pionic decays of hypernuclei. The method is powerful for lifetime measurements — the result of $\tau = 220^{+50}_{-40}$ ps was obtained by using statistics of 25 events [45] and include statistical errors only because there were no systematic errors.

However, disadvantages of the approach should be noted as well. The trigger tuned to register only pionic decays is not effective to register hypernuclei with $A \geqslant 12$ because the branching ratio of the pionic decay drops till 5–10% for carbon hypernuclei and decreases quickly for heavier hypernuclei. Moreover, the trigger tuned to register a narrow class of daughter nuclei with $Z + 1$ protons, puts a limit on a list of hypernuclei which can be investigated because some hypernuclei have no daughter nuclei of this type. Of course, a more universal trigger can be used (as it is suggested for the program of nonmesonic decays in the future Dubna experiments) to solve this restriction. It should be noted that in the Dubna experiments the hypernuclei decays are registered and investigated for a long period of time after the production moment when nuclei have been de-excited to the ground level, that is why it is impossible to use the method for the spectroscopy of production levels. On the other hand, in some cases there is a possibility to measure excitation levels of the daughter nuclei which can give information on decay processes i.e., on the weak ΛN interactions. For example, a possibility to measure excitation levels of ^{8}Be, which is a part of a specific hypernuclear decay chain, is quite realistic. (Below this problem will be discussed in detail.)

Meanwhile, the experiments at the Synchrophasotron beams were interrupted because the data collection rate was rather low due to the low accelerator duty cycle and the large memory time of the streamer chamber. Since the short Synchrophasotron spill time does not exceed 0.5 s one should wait for 8–9 s till

the next spill is accelerated and extracted. On the other hand, the beam intensity should be limited at the level of 10^5 s^{-1}, otherwise the streamer chamber is overloaded with «old» interactions and tracks due to its memory time of 3–5 μs.

6.3. New Programme. Last few years, the Nuclotron [100], a new superconductive accelerator at the Laboratory of High Energies (JINR), has been developed step by step to reach all of the designed specifications. The ultimate peak beam energy of this machine is 12 GeV for protons and 6 GeV/nucleon for nuclei with $Z/A = 1/2$. The accelerator is generally used as a source of medium energy nuclear beams. The top aim is to obtain the relativistic uranium beam. The secondary tritium beams are expected to be also produced. However, the main stream of the approved research program [101] for the next 3–5 years includes experiments with light and medium nuclear beams as well as polarized deuteron beams. There was a large delay between the first accelerated beam in 1994 and the first successful test of the beam extraction system and a first experiment in the extracted beam in March 2000, that was a crucial moment in the Nuclotron progress. For example, the beam extraction efficiency was increased up to 60–70% in this run. At the end of 2000, efficiency of a helium refrigerator was improved to overcome the run duration limit of ten days due to insufficient power of the liquid nitrogen factory. Now a Nuclotron run can be prolonged for any time necessary for experiments. The annual running time of the Nuclotron is 2000–2500 h per year. So, the Nuclotron can be nominated now as an actually operating machine. Table 9 represents some Nuclotron beam properties (available at the middle of 2004) essential for the hypernuclear experiments. It should be

Table 9. **Nuclotron parameters in summer of 2004 in comparison with the design values**

Parameter	Designed	Achieved
$E_{\max}$, GeV/A	6.0	4.1
Accelerated nuclei	p, d,..., ^{238}U	p, d, ^{4}He, Li, B,^{12}C, ^{14}N, ^{16}O, ^{24}Mg, ^{40}Ar, ^{56}Fe, ^{84}Kr
Flat top duration of beam, s	>10	10
Spill of the extracted beam, s	$8-10$	10
~ 5 Magnetic field (max), T	2.1	1.5
Beam intensity: p	$\sim 1 \cdot 10^{11}$	$3 \cdot 10^{10}$
d	$\sim 1 \cdot 10^{11}$	$3 \cdot 10^{10}$
^{4}He	$\sim 5 \cdot 10^{11}$	$5 \cdot 10^{8}$
^{12}C	$\sim 5 \cdot 10^{9}$	$5 \cdot 10^{9}$
^{56}Fe	$2 \cdot 10^{8}$	$2.5 \cdot 10^{6}$

taken into account that the Nuclotron beams are improved from run to run. The Nuclotron beams offer new possibilities for the hypernuclear experiments. In future experiments the data collection rate can be gained by more than 2 orders

(in comparison with experiments [45] at the Synchrophasotron) with an expected excellent Nuclotron duty cycle and proportional chambers instead of the streamer chamber. That is why an extended hypernuclear research programme [102–104] was offered for the SPHERE spectrometer [105]. It was aimed to carry out experiments similar to the previous Dubna experiments with significantly higher statistics and to open new items as well. Since the first experiments will be based on the well-known experimental conditions with the trigger tuned to match mesonic decays of the lightest hypernuclei, the possibility to investigate non-mesonic decays in the Nuclotron beams has been also discussed [91].

Considering the very first hypernuclear experiments offered for the SPHERE spectrometer, let us note lifetime measurements for the lightest hypernuclei ${}^{4}_{\Lambda}$H and ${}^{3}_{\Lambda}$H produced in ^{4}He or ^{3}He beams. In comparison with the previous Dubna experiments the main innovation is much higher available statistics. Indeed, if 25 events were observed in the previous experiment, 400–600 events per day are expected if the suggested trigger manages with 10^6 s^{-1} ^{4}He or ^{3}He beams. It means that lifetimes can be measured within 2–3% statistical errors.

Such a high intensity hypernuclear beam allows one to investigate interactions of hypernuclei with a medium. For example, a substantially new method to determine the binding energy of ${}^{3}_{\Lambda}$H (${}^{6}_{\Lambda}$He is also a perspective case of low binding energy) — the Z dependence of the Coulomb dissociation cross section of hypernuclei was proposed.

The hypertritium Coulomb dissociation on the nuclei of different electric charge will provide information on ${}_{\Lambda}$B. The Coulomb dissociation cross section [106, 107] of a weakly bound hypernucleus is inversely proportional to the value of binding energy and directly proportional to the square of the target nucleus charge (see, for example, [107] where $\sigma_d^C \sim Z^{1.92}$). Estimations predict that the 10% accuracy of measuring the dissociation cross section at the Nuclotron is quite realistic. On the other hand, the Coulomb dissociation cross section on a U target changes from a few barns to 60 b if the binding energy of Λ in the hypertriton drops from 0.15 to 0.01 MeV. The possibility to estimate the binding energy using this method is especially attractive in case of a very low value of the binding energy when a traditional kinematic analysis is quite difficult.

It should be noted that different absorbers will be used in the experiments, thus allowing one to investigate the model itself and, perhaps, providing some details of Λd and ΛN interactions [107] because the model calculations are performed for different absorbers as well. The Coulomb dissociation cross section will be measured by comparison of the hypernuclear beam intensity beyond different absorbers (to count survive hypernuclei) and there is no idea to identify (to count) products of dissociation. It should be also mentioned that the nuclear part of total cross sections can be measured experimentally and then subtracted because Coulomb dissociation is negligible (Z^2 dependence) in case of light absorbers.

Since experiments at ^{4}He or ^{3}He beams are scheduled for the pionic decays of the lightest nuclei with the trigger well tested in the previous experiments, the investigation of nonmesonic decays is estimated as much more complicated and difficult. Two problems should be noted — trigger background and minimal trigger rate are expected much higher and higher resolution track detectors should be used.

At high-energy nuclear beams one can observe hypernuclear production described generally by a scheme

$$^{Z}A + A_{\rm targ} \to {}^{Z-i}_{\Lambda}(A-k) + \dots \tag{10}$$

where $i, k = 0, 1, \dots$ For example, in ^{12}C beam a set of hypernuclei ($^{12}_{\Lambda}$C, $^{11}_{\Lambda}$C, $^{10}_{\Lambda}$C, $^{11}_{\Lambda}$B, $^{10}_{\Lambda}$B, etc.) can be produced (see [95, 96]). By the way, in other interactions different ^{12}C fragments are produced copiously. So, one should care of a more sophisticated trigger in this case. Problems of isotope identification are also more essential than in case of the lightest hypernuclei. On the other hand, one can use nontrivial beams to produce specified hypernuclei. For example, ^{10}B beam can be used to produce $^{10}_{\Lambda}$B hypernuclei in order to simplify identification and to reduce background events (but, maybe at lower production cross section and higher background trigger rate). In the process of discussion on the future programme it has been shown [75] that the study of the specified nonmesonic decays containing intermediate $^8\mathrm{Be} \to \alpha + \alpha$ will provide unique data on the properties of weak ΛN interaction. In the meantime it was noted that high resolution detectors [108] should be added to the proportional chambers to carry out these very interesting and difficult experiments of the Dubna hypernuclear programme; it seems that the Nuclotron beams and the SPHERE spectrometer will provide a possibility to obtain the desired result.

The layout of the hypernuclear experiment (the SPHERE spectrometer adjusted for hypernuclear experiments) see in Fig. 9 (mesonic decays of light hypernuclei) and Fig. 10 (nonmesonic decays). The SPHERE spectrometer is designed as a rather universal spectrometer therefore «hypernuclear» detectors are presented here without other targets, hodoscopes, counters, etc.

Figures 9 and 10 display only these detectors which will be used for the first hypernuclear experiments, in part, for the experiment dedicated to investigate Coulomb dissociation of the hypertritium nuclei in the absorber noted by A. Incident He beam (6.8 GeV/c per nucleon) interacts with a carbon target (T) 10–15 cm long, and hypernuclei of 6.2–6.7 GeV/c per nucleon momentum (see Fig. 7) are produced with a cross section of microbarns [95,96]. The mean decay range of hypernuclei is approximately 40 cm. So, one can insert a trigger counters C_1 just near the target to measure the charge value of hypernucleus while a block of trigger detectors C_2 beyond the decay volume (V) measures the charge of the decay products. In the first experiments proportional chambers $PC_{1,2}$ will be used

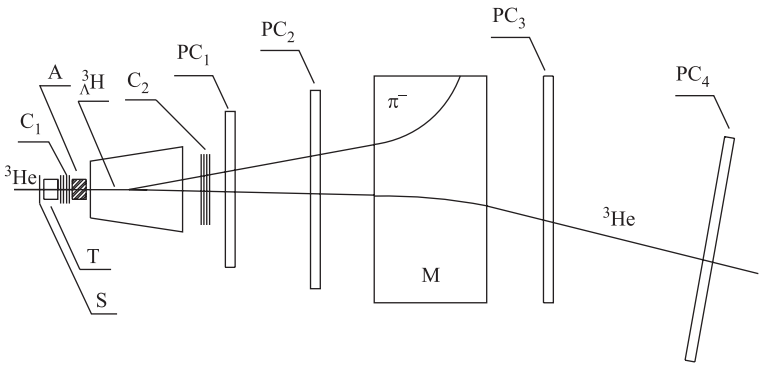

Fig. 9. SPHERE spectrometer adapted for the first hypernuclear experiments, for example, for ${}^{3}_{\Lambda}$H production in a ^{3}He beam and subsequent electromagnetic dissociation in different absorbers. T — target; A — absorber for studying Coulomb dissociation of ${}^{3}_{\Lambda}$H hypernuclei; S, $C_{1,2}$ — trigger counters; V — vacuum decay volume; M — magnet; PC_{1-4} — proportional chambers

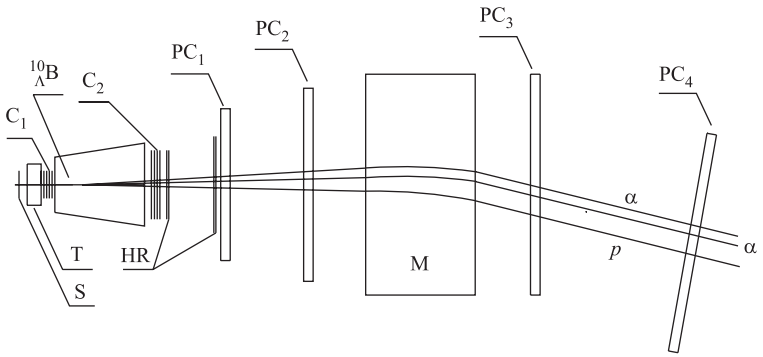

Fig. 10. SPHERE spectrometer modified to investigate the nonmesonic decay of ${}^{10}_{\Lambda}$B produced in the Nuclotron carbon beam. S — the beam control counters; T — target; $C_{1,2}$ — the trigger Cherenkov counters; V — vacuum decay volume; HR — high resolution detectors; M — magnet; PC_{1-4} — proportional chambers

as trackers to locate the hypernuclear decay points. For more complicated experiments the high resolution track detectors (HR) will be installed between the decay volume V and the first of the proportional chambers H_1 to measure coordinates and to locate vertex position of the decay products emitted at very small angles (see Fig. 8). Obviously, if the decay point is located inside the vacuum decay volume, there is no doubt that the decay of a hypernucleus has been registered. The proportional chambers $PC_{3,4}$ beyond the analyzing magnet together with the

chambers $PC_{1,2}$ measure momenta of positive secondary particles (daughter nuclei and fragments) to identify different hypernuclear isotopes, if necessary. Also it should be noted that in all experiments the distance between target T and decay volume V can be reduced to 1–3 cm (20–25 cm in the previous experiments) due to thin (1–4 mm) radiators of Cherenkov detectors. Except, of course, the experiment of hypernuclei dissociation in absorber A.

However, one should note that proportional chambers are a good enough tracker for mesonic decays of light hypernuclei ($^{4}_{\Lambda}$H) because less than 2–3% of events are lost if the chambers are placed at a short distance of 10–15 cm beyond the decay volume. There are two reasons why hypernuclear events can be lost due to track detectors. The first one is overlapping tracks when the secondary particle (for example, pion and daughter nucleus) hits are registered as one cluster in the proportional chambers. The other reason is the track direction measuring errors, that sometimes does not allow one to locate a decay vertex undoubtedly. If there is a probability that the vertex is located in the target, in the trigger detector or at the window of the vacuum volume, the event should be rejected. The Monte-Carlo calculations have shown that the efficiency for pionic decays is close to 100% if the proportional chambers are moved at a distance of 20–30 cm beyond the decay volume. One should take into account that increasing the distance between the decay volume and the first (nearest) track detector decreases the accuracy of the vertex location. However, negative pions are generally emitted at quite large angles and there are no serious problems to check that the decay point is located inside the decay volume and interactions in the target or counters cannot be interpreted as hypernuclear decays. Just on the contrary, high resolution detectors (see HR in Fig. 10) should be used to register nonmesonic decays with a sufficient efficiency.

6.4. Nonmesonic Decays. It was noted above that the trigger scheduled to investigate the mesonic decay mode is adequate for a limited set of hypernuclear production and decay chains. Sometimes there do not exist stable daughter nuclei to be registered by the trigger. Considering nonmesonic decays of hypernuclei, naturally, one must take into account that for any specified production and decay scheme a special optimized trigger should be elaborated and tuned.

Let us analyze a possibility to investigate a special case of nonmesonic decay of hypernuclei (for example $^{10}_{\Lambda}$B). It can decay as $^{10}_{\Lambda}\mathrm{B} \rightarrow n + p + {}^{8}\mathrm{Be}$ with subsequent ^{8}Be decay emitting two α's within a very small angle. One meets two problems in the case — a serious trigger background and detector resolution when two α's, emitted within a narrow angle, hit the detector at a short distance and can be registered as one hit or a cluster. The Monte-Carlo simulation and analysis have shown [108] that proportional chambers are not an adequate device in this case because practically all α's in the first proportional chambers will activate one cluster response. There is no profit to shift the detector at a larger distance beyond the decay volume because the accuracy of vertex location drops very quickly. A detector (scintillating fibers or a silicon microstrip

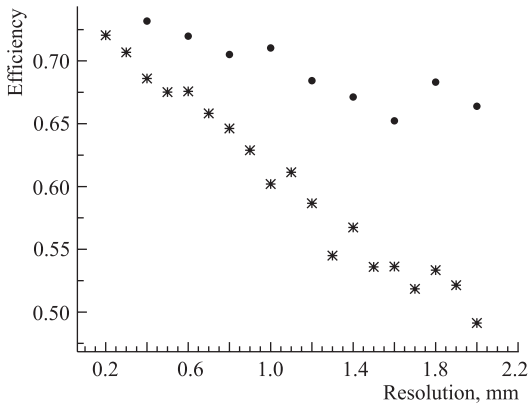

Fig. 11. Tracker efficiency vs. resolution of the high resolution detectors. • — a detector at a distance of 5 cm beyond the decay volume; ∗ — a detector at a distance of 45 cm

detector) of a sufficiently high resolution should be used to register a reasonable number of hypernuclear events (see Fig. 11). The same simulation has shown that the size of a high resolution detector should not be too large — 6×6 and 12×12 cm (see Fig. 12).

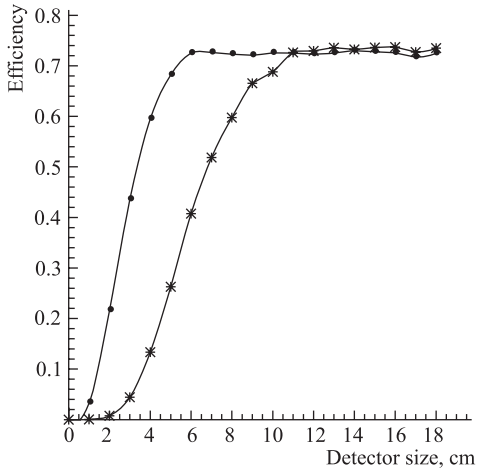

Fig. 12. Tracker efficiency vs. size of the high-resolution detectors. • — a detector at a distance of 5 cm beyond the decay volume; ∗ — a detector at a distance of 45 cm

If 0.4 mm scintillating fibers are used, the number of lost events can be reduced to a level of 2–3% while 30–40% of decays will be lost if the resolution of the first detector is 2 mm. If the second detector is situated at a distance of 30–50 cm from the first one, the resolution of the second detector may be of the order of 1 mm. In Fig. 11 the tracker efficiency is presented as a function of the resolution value for the scintillation fiber or Si microstrip detectors.

If one chooses a reasonable resolution value (0.4 mm for the first nearest detector at a distance of 5 cm beyond the decay volume and 1 mm for the second one at a distance of 40 cm beyond the first one) it is quite easy to estimate the minimal size of the detectors (see Fig. 12).

If the first detector is installed just beyond the decay volume, the event losses due to uncertain location of the decay vertex are minimal while losses due to unresolved hits are maximal. It seems that the best position for the first detector is 5–15 cm beyond the decay volume. At this detector position 15% of events will be lost due to the uncertain vertex reconstruction (if the high-resolution detector pitch size is 0.4 mm). If the pitch size is reduced to 0.2 mm, the losses are reduced to 0–1%. Efficiency of 75% calculated in Fig. 11 is limited by geometrical cuts (hypernuclear decays before the «sensitive» part of the decay volume). Let us note again that such a detector resolution solves the problem of overlapping tracks as well.

The trigger problem is most serious in the experiments dedicated to the study of the nonmesonic decays of hypernuclei. It was noted above that in case of mesonic decays the trigger detectors can register the daughter nuclei with a charge value larger than that of hypernuclei (detector signals proportional to $(Z+1)^2$ and Z^2, correspondingly) and beam fragments cannot simulate the $(Z+1)^2$ signal. Meanwhile, a lot of beam fragments ejected from the target or from the trigger detectors can simulate signals of the nonmesonic decay products. The most difficult problem is the beam fragments from the edge of the trigger detector placed before the decay volume (for example, from counters C_1, see Fig. 10). The trigger electronics is tuned to detect counter C_1 response corresponding to the signal from specified hypernucleus. For example, a hypernucleus ${}^{10}_{\Lambda}$B should produce a signal of the amplitude proportional to 25 (square of $Z = 5$). However, a boron nucleus — a fragment of a beam carbon nucleus — will give similar response in the counters C_1. The general part of these fragments will be ignored by the trigger electronics because it should be tuned to find out among the counter C_2 signals the amplitudes proportional to 9 — a superposition of response to alpha-alpha-proton (decay products of ${}^{10}_{\Lambda}$B) which is equal to $2^2 + 2^2 + 1^2 = 9$. Unfortunately, a nonzero fraction of fragments — boron nuclei — can interact at the edge of the last counter of group C_1 or the first counter of group C_2 to produce the same particles and counter signals which are expected in the decay of ${}^{10}_{\Lambda}$B. If the fragmentation of boron takes place at a short distance of the detector C_1 edge the response of the C_1 is not distorted significantly. The higher is the resolution of counter (detector) C_1, the thinner is the layer of this detector which can simulate a signal of the nonmesonic hypernuclear decay. But this layer cannot be equal to zero because the detector resolution is a finite value. Unfortunately, the counter resolution increases proportionally to the square root of the counter thickness while fragmentation is proportional to the thickness.

It seems that there is no way to reduce the background triggers for non-mesonic decays to zero level. So, the task is to eliminate the background trigger rate till the capability of the track detector readout system. In this case all hyper-nuclear triggers will be registered by track detector readout system and off-line analysis will reject background events. One should use counters of different

thickness to have the high resolution and to minimize fragmentation effects. For example, two or three Cherenkov counters with thick quartz radiators can be used in each group $C_{1,2}$ to reach high resolution and to find out a signal of a specified reaction. An additional counter with a thin (1 mm) quartz radiator eliminates fragmentation effects.

Figures 13 and 14 present the results of calculation based on the data obtained in 2003 when a Cherenkov counter with a 1 mm quartz radiator was tested at the Nuclotron carbon beam. The beam energy was 2.3 GeV/nucleon. One can hope that at 6 GeV energy the resolution of counters and background suppression will be better. The calculated response of a 1 mm quartz counter to ${}^{10}_{\Lambda}$B hypernuclei and to boron fragmentation in the quartz radiator shows (Fig. 13) that 70% fragmentation events can be eliminated by a 1 mm counter. On the other hand, the total number of expected fragmentation events in 1 mm of quartz is not too large and in the result the number of the background triggers provoked by boron fragmentation in the trigger counter will not exceed 20–30 s^{-1} if a carbon beam of 10^6 s^{-1} is used to produce hypernuclei. Another picture (Fig. 14) proves that the 1 mm counter will reject fragments produced in «thick» counters — indeed, the threshold tuned to register all hypernuclei is too high for the signals of fragments born in «thick» radiators.

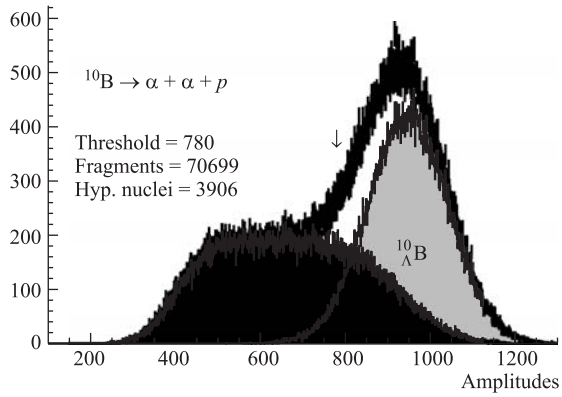

Fig. 13. Response of a 1 mm quartz radiator Cherenkov counter to ${}^{10}_{\Lambda}$B hypernuclei (grey histogram) and fragmentation of boron nuclei (black histogram) in the radiator. If a proper threshold (ampl. = 780) is chosen, approximately 71% of fragment signals are lower than the threshold while only 4% hypernuclei will be rejected. 100000 entries for each histogram, sum of two is also displayed. The arrow shows a possible threshold level

Of course, one can discuss different approaches to solve the trigger problem. For example, there was an idea to use Si dE/dx detectors, placed before and after the vacuum decay volume [91]. Obviously, such a detector can be very thin

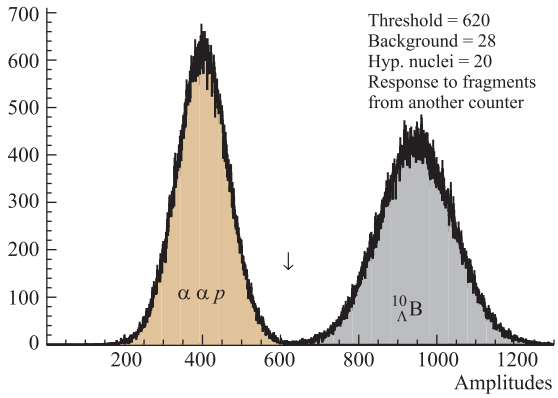

Fig. 14. Response of a 1 mm quartz radiator Cherenkov counter to $^{10}_{\Lambda}$B hypernuclei and fragmentation of boron nuclei in other counters. Signals can be easy separated. 100000 entries for each histogram

(0.4–0.5 mm). However, one should use very sophisticated electronics to manage with high intensity (10^6 s^{-1}) beam of carbon and fragments. Sometimes quite different approaches are discussed. For example, an idea to count a number of particles before and beyond the decay volume or to locate the origin of tracks leaving the decay volume. Such a trigger can be used if one has high resolution detectors (let us remember, that two α's are ejected at a narrow separation angle) to count particles or to estimate the vertex position using the tracks which are almost parallel to the beam direction. It seems that the trigger of such a type can be used as a trigger of the second level to manage with a high intensity beam. Anyway, a trigger based on Cherenkov counters seems to be the simplest one.

So, meanwhile the experimental investigation of nonmesonic decays of boron hypernuclei is not easy to carry out. One can solve the task by using an adequate trigger to reject the background triggers and high resolution tracker to locate the decay vertex position.

Our analysis of the Dubna experiment proposal has shown that investigations of the high energy hypernuclei will shed light on essential weak-interaction problems. The expected data will be complementary to that obtained at the experiments with target nuclei excitation and will enlarge significantly our knowledge on the properties of hypernuclei, especially on ΛN weak interactions. The method is perspective and can be extrapolated to higher beam energies. While Dubna experiments will be carried out at nuclear beams up to 10^6 nuclei/s, experiments at 10^9–10^{10} nuclei/burst were discussed by A. Sakaguchi at the International Workshop on Nuclear and Particle Physics at 50 GeV PS [109]. High energy beam (25 GeV/u) allows one to use long (10 m) magnet separation system beyond

the target to dump the beam of nuclei and to have separated hypernuclear beam (approximately 1 hypernucleus per burst or 10^4 per day!).

7. WHAT WILL ALPHA DECAYS TELL US ABOUT?

We have to simplify expression (4) for partial decay width Γ_i^τ in order to compensate a small number of quantities measured at the Nuclotron. We have used the results of recent calculations [64,70]: the contribution of the decay rates from the $N\Lambda$ relative P state is only $\approx 5\%$ of the total decay rates for the ${}^{12}_{\Lambda}\mathrm{C}$ hypernucleus, so we neglect them for a moment. Now we can write an extremely simple expression for $\tilde{\Gamma}_i^\tau$

$$\tilde{\Gamma}_i^\tau = \nu_i \varepsilon_1^2 \beta_0 [G_i^{(0)} R_{\tau 0} + G_i^{(1)} R_{\tau 1}]. \tag{11}$$

Here, β_0 and ε_1 stems from Talmi–Moshinsky transformation

$$\Psi^{N\Lambda} = \mid p_N s_\Lambda : {}^{2S+1}P_J\rangle = \sqrt{\beta_0} \mid \Phi_{11}(\mathbf{R})\varphi_{00}(\mathbf{r}) : {}^{2S+1}P_J\rangle + \\ + \sqrt{\beta_1} \mid \Phi_{00}(\mathbf{R})\varphi_{11}(\mathbf{r}) : {}^{2S+1}P_J\rangle,$$

$\varepsilon_0 \equiv \langle \mathrm{e}^{i\mathbf{PR}} \mid \Phi_{00}(\mathbf{R})\rangle$ and $\varepsilon_1 \equiv \langle \mathrm{e}^{i\mathbf{PR}} \mid \Phi_{11}(\mathbf{R})\rangle$ and $R_{\tau S}$ are well-known rates for the spin-singlet ($R_{\tau 0}$) and spin-triplet ($R_{\tau 1}$) elementary $\tau\Lambda \to \tau\, n$ interaction introduced by Dalitz and Block [85].

We also rewrite the spectroscopic factor for $N\Lambda$ pair as

$$G_{\mathcal{J}}\left(\{c\},\{i\},\tau LSJ\right) = \nu_i (G_i^{(0)} + G_i^{(1)}),$$

with $G_i^{(0)}$ and $G_i^{(1)}$ for weight of the singlet and triplet state in the wave function.

The benefit of such oversimplification is a possibility to relate decay rates for $A = 10$ hypernuclei to decay rates for s-shell hypernuclei (${}^4_\Lambda\mathrm{H}$ and ${}^4_\Lambda\mathrm{He}$), where sophisticated calculations were published recently [56, 64] and phenomenological analysis exists for some decades, most recent one [86] (see references therein).

$$\Gamma^n_{\mathrm{H}} = R_{n0} + 3R_{n1}, \quad \Gamma^p_{\mathrm{H}} = 2R_{p0},$$
$$\Gamma^n_{\mathrm{He}} = 2R_{n0}, \qquad \Gamma^p_{\mathrm{He}} = R_{p0} + 3R_{p1},$$

$\Gamma^\tau_{\mathrm{H}} \equiv \Gamma^\tau({}^4_\Lambda\mathrm{H})k^{-1}$, $\Gamma^\tau_{\mathrm{He}} \equiv \Gamma^\tau({}^4_\Lambda\mathrm{He})k^{-1}$, $k = \rho/6$, ρ being nuclear density.

$$\frac{R_{n0}}{R_{p0}} = \frac{\Gamma^n_{\mathrm{He}}}{\Gamma^p_{\mathrm{H}}}, \quad \frac{R_{n1}}{R_{n0}} = \frac{1}{3}\left[2\,\frac{\Gamma^n_{\mathrm{H}}}{\Gamma^n_{\mathrm{He}}} - 1\right], \quad \frac{R_{p1}}{R_{p0}} = \frac{1}{3}\left[2\,\frac{\Gamma^p_{\mathrm{He}}}{\Gamma^p_{\mathrm{H}}} - 1\right].$$

Table 10. **Ratios $\gamma_i^{n/p}$ (see (12)) for different models of weak interaction**

Model		$A=4$			$A=10$	
		R_{n0}/R_{p0}	R_{n1}/R_{n0}	R_{p1}/R_{p0}	$\gamma_1^{n/p}$	$\gamma_2^{n/p}$
TPE [64]:	V_π	2.0	1.0	27.0	0.14	0.08
	$+V_{2\pi/\rho}$	2.5	2.6	35.0	0.25	0.19
	$+V_\omega$	2.0	0.57	10.0	0.28	0.14
	$+V_{2\pi/\sigma}$	2.0	0.39	3.40	0.63	0.28
HQ [56]:	π	2.0	0.54	15.0	0.19	0.09
	$\pi + K$	1.8	4.6	19.0	0.50	0.44
	DQ	0.85	1.3	0.74	1.12	1.41
	All	0.13	26	4.40	0.65	0.75
OME [65]:	π	2.0	0.7	12.1	0.25	0.13
	PS	2.0	7.6	30.0	0.56	0.51
	PS + PV	2.0	35	21.3	3.22	3.26
Phenomenological [86]:						
	AG1	0.6	2.2	1.2	0.87	1.06
	AG2	2.0	2.2	5.0	1.07	0.90

The ratios

$$\gamma_i^{n/p} \equiv \frac{\tilde{\Gamma}^n_{\alpha\alpha i}\,(^{10}_{\Lambda}\mathrm{Be})}{\tilde{\Gamma}^p_{\alpha\alpha i}\,(^{10}_{\Lambda}\mathrm{B})} = \frac{R_{n0}}{R_{p0}}\,\frac{G_i^{(0)} + (1-G_i^{(0)})(R_{n1}/R_{n0})}{G_i^{(0)} + (1-G_i^{(0)})(R_{p1}/R_{p0})}. \qquad (12)$$

Clearly, the ratio $\gamma_i^{n/p}$ is very sensitive to the model of the weak interaction (see Table 10).

CONCLUSION

Due to their salient cluster structure — $\alpha\alpha$ $N\Lambda$ — it may be possible to measure in the $^{10}_{\Lambda}$Be and $^{10}_{\Lambda}$B hypernuclei *several* partial «alpha-decay widths» $\Gamma^{\tau}_{\alpha\alpha i}$, corresponding to different states of the residual nucleus $^8\mathrm{Be}^*(E_i;\, J_i^\pi,\, T_i)$ which decays through the $\alpha\alpha$ channel. In such a way we can determine *one-nucleon stimulated* process $\Lambda N \to nN$ unambiguously. Obviously, the role of the two-nucleon stimulated process $\Lambda np \to nnp$ could be seen by detection of α particles in the decay of the hypernucleus $^{11}_{\Lambda}\mathrm{B} \to {}^8\mathrm{Be} + nnp$.

The energy of α particles determines the final state of the residual nucleus ^{8}Be, its quantum numbers, hence also the actual weight of the four possible wave functions of the $N\Lambda$-pair: $p_{\frac{1}{2}}s_\Lambda$ with $J = 0, 1$ and $p_{\frac{3}{2}}s_\Lambda$ with $J = 1, 2$. In

an ideal case when the transitions to final states with $J_i = 0, 1, 2$, and 3 are observed, one can unambiguously determine all four matrix elements $w_{\ell\tau}^{SJ}$. These matrix elements $w_{\ell\tau}^{SJ}$ will open up a possibility to extend the phenomenological model by Block & Dalitz up to p-shell hypernuclei.

The extended hypernuclear research programme was offered for the SPHERE spectrometer. The first experiments will be based on the well-known experimental conditions with the trigger tuned to match mesonic decays of the lightest hypernuclei. When the high resolution detectors will be added to the proportional chambers the Nuclotron beams and SPHERE spectrometer will provide a possibility to carry out investigation of nonmesonic decays of ${}^{10}_{\Lambda}$Be and ${}^{10}_{\Lambda}$B hypernuclei.

The ratio $\gamma_i^{n/p}$ is very sensitive to the model of the weak interaction. But this ratio reveals a small sensitivity to the choice of nuclear residual interaction employed in the calculations. So, even the first results which can be expected from the Nuclotron will be of a great value.

Acknowledgements. We are grateful to J. Bartke, T. Bressani, K. Itonaga, S. Khorozov, A. Kovalenko, V. Kuz'min, R. Mach, J. Mareš, A. Margaryan, T. Motoba, A. Parreño, A. Ramos, and Liguang Tang for many constructive discussions. The work of L. M. has been supported by grant 202/02/0930 of the Grant Agency of Czech Republic. The work of J. L. has been supported in part by RFBR grant 99-02-17655.

REFERENCES

1. *Danysz M., Pniewski J.* // Bull. Acad. Polon. Sci. 1952. V. 3. P. 42;
   Danysz M., Pniewski J. // Phil. Mag. 1953. V. 44. P. 348.
2. *Gell-Mann M.* // Phys. Lett. 1964. V. 8. P. 214.
3. *Holzenkamp B., Holinde K., Speth J.* // Nucl. Phys. A. 1989. V. 500. P. 483;
   Holinde K. // Nucl. Phys. A. 1992. V. 547. P. 255c;
   Reuber A. G., Holinde K., Speth J. // Czech. J. Phys. 1992. V. 42. P. 1115;
   Haidenbauer J., Melnitchouk J. W., Speth J. // Proc. of the Intern. Conf. «Mesons and Light Nuclei», Prague, 2001. AIP Conf. Proc. N. Y., 2001. V. 603. P. 421.
4. *Rijken Th. A.* // Nucl. Phys. A. 2001. V. 691. P. 322c;
   Rijken Th. A. // Nucl. Phys. A. 1998. V. 639. P. 29c.
5. *Hao J. et al.* // Phys. Rev. Lett. 1993. V. 71. P. 1498.
6. *Yamamoto Y. et al.* // Czech. J. Phys. 1992. V. 42. P. 1249.
7. *Gal A., Soper J. M., Dalitz R. H.* // Ann. Phys. 1978. V. 113. P. 79;
   Millener D. J. et al. // Phys. Rev. C. 1985. V. 31. P. 449;
   Fetisov V. N. et al. // Z. Phys. A. 1991. V. 339. P. 399.
8. *Miyagawa K., Glöckle W.* // Phys. Rev. C. 1993. V. 48. P. 2576;
   Miyagawa K. et al. // Phys. Rev. C. 1995. V. 51. P. 2905;
   Miyagawa K. et al. // Few-Body Systems Suppl. 2000. V. 12. P. 324.

9. *Davis D. H., Pniewski J.* // Contemp. Phys. 1986. V. 27. P. 91;
   Davis D. H., Sacton J. High Energy Physics. N. Y.: Academic Press, 1967. V. 2.
10. *Podgoretsky M. I.* // Zh. Eksp. Teor. Fiz. 1963. V. 44. P. 695.
11. *Bressani T., Fainberg A.* // Proc. Summer Study Meeting. BNL 50579. 1976. P. 137;
    Bonazzola G. C. et al. // Phys. Lett. B. 1974. V. 53. P. 297;
    Bonazzola G. C. et al. // Phys. Rev. Lett. 1975. V. 34. P. 683.
12. *Bruckner W. et al.* // Phys. Lett. B. 1975. V. 55. P. 107;
    Bruckner W. et al. // Phys. Lett. B. 1976. V. 62. P. 481;
    Povh B. // Ann. Rev. Nucl. Part. Sci. 1978. V. 28. P. 1.
13. *Chrien R. E., Dover C. B.* // Ann. Rev. Nucl. Part. Sci. 1989. V. 39. P. 113.
14. *Milner C. et al.* // Phys. Rev. Lett. 1985. V. 54. P. 1237.
15. *Hasegawa T. et al.* // Phys. Rev. C. 1996. V. 53. P. 1210.
16. *Ajimura S. et al.* // Phys. Lett. B. 1992. V. 282. P. 293.
17. *Hungerford E. V.* // Nucl. Phys. A. 2001. V. 691. P. 21c;
    Miyoshi T. et al. // Phys. Rev. Lett. 2003. V. 90. P. 232502.
18. *Bandō H., Motoba T., Žofka J.* // Intern. J. Mod. Phys. A. 1990. V. 5. P. 4021.
19. *Tamura H. et al.* // Phys. Rev. Lett. 2000. V. 84. P. 5963;
    Tanida K. et al. // Phys. Rev. Lett. 2001. V. 86. P. 1982;
    Tamura H. // Nucl. Phys. A. 2001. V. 691. P. 86c.
20. *Greiner W.* // Intern. J. Mod. Phys. E. 1996. V. 5. P. 1.
21. *Schaffner-Bielich J. et al.* // Phys. Rev. Lett. 2002. V. 89. P. 171101.
22. *Zenoni A.* // Nucl. Phys. A. 1999. V. 654. P. 96c.
23. *Feliciello A. (for the FINUDA Collab.)* // Nucl. Phys. A. 2001. V. 691. P. 170c.
24. *Grzonka D., Kilian K.* // Nucl. Phys. A. 1998. V. 639. P. 569c.
25. *Cohen J.* // Progr. Part. Nucl. Phys. 1990. V. 25. P. 139.
26. *Oset E., Ramos A.* // Progr. Part. Nucl. Phys. 1998. V. 41. P. 191.
27. *Alberico W. M., Garbarino G.* // Phys. Rep. 2002. V. 369. P. 1.
28. *Okun' B. L.* Leptons and Quarks. M.: Nauka, 1990;
    Donoghue J. F. et al. // Phys. Rep. 1986. V. 131. P. 319;
    Vainshtein A. I. et al. // Zh. Eksp. Teor. Fiz. 1977. V. 72. P. 1275.
29. *Hagiwara K. et al. (Particle Data Group)* // Phys. Rev. D. 2002. V. 66. P. 010001.
30. *Dubach J. F.* // Nucl. Phys. A. 1986. V. 450. P. 71c;
    Dubach J. F. et al. // Ann. Phys. 1996. V. 249. P. 146.
31. *Bhang H. et al.* // Phys. Rev. Lett. 1998. V. 81. P. 4321.
32. *Kulessa P. et al.* // Phys. Lett. B. 1998. V. 427. P. 403.
33. *Park H. et al.* // Phys. Rev. C. 2000. V. 61. P. 054004.
34. *Kamys B. et al.* // Eur. Phys. J. A. 2001. V. 11. P. 1.
35. *Kulessa P. et al.* // Acta Phys. Polon. B. 2002. V. 33. P. 603.
36. *Cassing W. et al.* // Eur. Phys. J. A. 2003. V. 16. P. 549.
37. *Alberico W. et al.* // Phys. Rev. C. 2000. V. 61. P. 044314.
38. *Jido D., Oset E., Palomar J.* // Nucl. Phys. A. 2001. V. 694. P. 525.

39. *Itonaga K. et al.* // Nucl. Phys. A. 1998. V. 639. P. 329c.
40. *Ramos A. et al.* // Phys. Rev. C. 1994. V. 50. P. 2314.
41. *Philips R., Schneps J.* // Phys. Rev. 1969. V. 180. P. 1307.
42. *Keyes G. et al.* // Nucl. Phys. B. 1973. V. 67. P. 29.
43. *Bohm G. et al.* // Nucl. Phys. B. 1979. V. 23. P. 93.
44. *Abdurakhimov A. et al.* // Nuovo Cim. A. 1989. V. 102. P. 645.
45. *Avramenko S. et al.* // Nucl. Phys. A. 1992. V. 547. P. 95c.
46. *Nield K. et al.* // Phys. Rev. C. 1976. V. 13. P. 1263.
47. *Grace R. et al.* // Phys. Rev. Lett. 1985. V. 55. P. 1055.
48. *Szymanski J. et al.* // Phys. Rev. C. 1991. V. 43. P. 849.
49. *Outa H. et al.* // Nucl. Phys. A. 1992. V. 547. P. 109c.
50. *Outa H. et al.* // Nucl. Phys. A. 1995. V. 585. P. 109c.
51. *Zeps V.* // Nucl. Phys. A. 1998. V. 639. P. 261c.
52. *Armstrong T. et al.* // Phys. Rev. C. 1993. V. 47. P. 1957.
53. *Noga V. et al.* // Ukr. Phys. J. 1990. V. 35. P. 171.
54. *Ohm H. et al.* // Phys. Rev. C. 1997. V. 55. P. 3062.
55. *Parreño A., Ramos A.* // Phys. Rev. C. 2002. V. 65. P. 015204.
56. *Sasaki K., Inoue T., Oka M.* // Nucl. Phys. A. 2002. V. 707. P. 477.
57. *Sakaguchi A. et al.* // Phys. Rev. C. 1991. V. 43. P. 73.
58. *Outa H. et al.* // Nucl. Phys. A. 1998. V. 639. P. 251c.
59. *Noumi H. et al.* // Proc. of Intern. Conf. «WEIN'95», Osaka, Japan, 1995. P. 550.
60. *Noumi H. et al.* // Phys. Rev. C. 1995. V. 52. P. 2936.
61. *Hashimoto O. et al.* // Phys. Rev. Lett. 2002. V. 88. P. 042503.
62. *Kim J. H. et al.* // Phys. Rev. C. 2003. V. 68. P. 065201.
63. *Satoh Y. et al.* // Phys. Rev. C. 2004 (submitted). Quoted in [62].
64. *Itonaga K., Ueda T., Motoba T.* // Phys. Rev. C. 2002. V. 65. P. 034617.
65. *Krmpotić F., Tadić F.* // Braz. J. Phys. 2003. V. 33. P. 187; nucl-th/0212040.
66. *Parreño A., Ramos A.* // Phys. Rev. C. 2002. V. 65. P. 015204.
67. *Barbero C. et al.* // Ibid. V. 66. P. 055209.
68. *Jido D., Oset E., Palomar J. E.* // Nucl. Phys. A. 2001. V. 694. P. 525.
69. *Outa H.* // Quoted in [73].
70. *Parreño A., Ramos A. Bennhold C.* // Phys. Rev. C. 1997. V. 56. P. 339.
71. *Alberico W. M. et al.* // Phys. Lett. B. 1991. V. 256. P. 134.
72. *Heddle D. P., Kisslinger L. S.* // Phys. Rev. C. 1986. V. 33. P. 608.
73. *Garbarino G., Parreño A., Ramos A.* // Phys. Rev. Lett. 2003. V. 91. P. 112501.
74. *Majling L., Batusov Yu.* // Yad. Fiz. 2001. V. 64. P. 1228.
75. *Majling L., Batusov Yu.* // Nucl. Phys. A. 2001. V. 691. P. 185c.
76. *Schooner J. L. et al.* // Nucl. Phys. A. 1971. V. 176. P. 567.

77. *Verba J. et al.* // Phys. Rev. 1967. V. 153. P. 1127.
78. *Towner I. S.* // Nucl. Phys. A. 1969. V. 126. P. 97.
79. *Bachelier D. et al.* // Ibid. P. 60.
80. *Barker F. C.* // Nucl. Phys. 1966. V. 83. P. 418.
81. *Cohen S., Kurath D.* // Nucl. Phys. A. 1968. V. 101. P. 1.
82. *Ajzenberg-Selove F.* // Nucl. Phys. A. 1988. V. 490. P. 1.
83. *Bennhold C., Ramos A.* // Phys. Rev. C. 1992. V. 45. P. 3017;
Ramos A. et al. // Nucl. Phys. A. 1992. V. 544. P. 783.
84. *Cohen J.* // Phys. Rev. C. 1990. V. 42. P. 2724;
Schumacher R. A. // Nucl. Phys. A. 1992. V. 547. P. 143c.
85. *Block M. M., Dalitz R. H.* // Phys. Rev. Lett. 1963. V. 11. P. 96.
86. *Alberico W. M., Garbarino G.* // Phys. Lett. B. 2000. V. 486. P. 362.
87. *Bohm G. et al.* // Nucl. Phys. B. 1974. V. 74. P. 237;
Zieminska D., Dalitz R. H. // Ibid. P. 248.
88. *Tang L. et al.* // Proc. of the Intern. Conf. «Mesons and Light Nuclei», Prague, 2001. AIP Conf. Proc. N. Y., 2001. V. 603. P. 173.
89. *Assamagan K. et al.* // Nucl. Instr. Meth. A. 1999. V. 426. P. 405.
90. *Podgoretskii M. I.* // Proc. of the Seminar «Nuclotron and Relativistic Nuclear Physics», Dubna, 1974. P. 81;
Okonov E. O. // Ibid. P. 104.
91. *Bartke J. et al.* // J. Phys. G. 1999. V. 25. P. 429.
92. *Mikhalev D. P. et al.* JINR Commun. P1-95-549. Dubna, 1995.
93. *Baltz A. J. et al.* // Phys. Lett. B. 1994. V. 325. P. 7.
94. *Asai F. et al.* // Phys. Lett. B. 1984. V. 143. P. 19.
95. *Wakai M. et al.* // Phys. Rev. C. 1988. V. 38. P. 748.
96. *Bandō H. et al.* // Nucl. Phys. A. 1989. V. 501. P. 900.
97. *Avramenko S. et al.* // Proc. of the XXIII Yamada Conf. «Nuclear Weak Process and Nuclear Structure», Osaka, 1989. Singapore, 1989. P. 468.
98. *Khorozov S.* Private communication.
99. *Kaptari L. P., Titov A. I.* // JETP Lett. 1979. V. 29. P. 375.
100. *Issinsky I. et al.* // Proc. of the Particle Accelerator Conf. IEEE. Vancouver, 1997. V. 1. P. 181.
101. Research Program of the Laboratory of High Energies. Dubna: JINR, 1999.
102. *Avramenko S. A. et al.* // JINR Rapid Commun. 1994. No. 5[68]. P. 14.
103. *Avramenko S. A. et al.* // Nucl. Phys. A. 1995. V. 585. P. 91c.
104. *Lukstins J.* // Nucl. Phys. A. 2001. V. 691. P. 491c.
105. *Afanasiev S. V. et al.* // JINR Rapid Commun. 1993. No. 3[93]. P. 40.
106. *Lyuboshitz V. L.* // Yad. Fiz. 1990. V. 51. P. 1013.
107. *Evlanov M. V. et al.* // Nucl. Phys. A. 1998. V. 632. P. 624.
108. *Golokhvastov A. I. et al.* // Proc. of the Intern. Conf. «Mesons and Light Nuclei», Prague, 2001. AIP Conf. Proc. N. Y., 2001. V. 603. P. 449.
109. *Sakaguchi A.* // Intern. Workshop «Nuclear and Particle Physics at 50 GeV PS», KEK, Tsukuba, Japan, 2001; www-jhf.kek.jp/NP01.
110. *Majling L., Kuz'min V. A., Tetereva T. V.* // Yad. Fiz. 2004. V. 67, No. 10.